Downlink OFDM-FAMA in 5G-NR Systems

Hanjiang Hong, *Member, IEEE*, Kai-Kit Wong, *Fellow, IEEE*, Hao Xu, *Senior Member, IEEE*, Yin Xu, *Senior Member, IEEE*, Hyundong Shin, *Fellow*, *IEEE*, Ross Murch, *Fellow*, *IEEE*, Dazhi He, *Senior Member, IEEE*, and Wenjun Zhang, *Fellow*, *IEEE*

***Abstract*—Fluid antenna multiple access (FAMA), enabled by the fluid antenna system (FAS), offers a new and straightforward solution to massive connectivity. Previous results on FAMA were primarily based on narrowband channels. This paper studies the adoption of FAMA within the fifth-generation (5G) orthogonal frequency division multiplexing (OFDM) framework, referred to as OFDM-FAMA, and evaluate its performance in broadband multipath channels. We first design the OFDM-FAMA system, taking into account 5G channel coding and OFDM modulation. Then the system's achievable rate is analyzed, and an algorithm to approximate the FAS configuration at each user is proposed based on the rate. Extensive link-level simulation results reveal that OFDM-FAMA can significantly improve the multiplexing gain over the OFDM system with fixed-position antenna (FPA) users, especially when robust channel coding is applied and the number of radio-frequency (RF) chains at each user is small.**

***Index Terms*—Fluid antenna multiple access (FAMA), fluid antenna system (FAS), OFDM, performance evaluation.**

I. Introduction

EXTREME massive connectivity is a cornerstone of massive machine-type communication (mMTC) in the fifth-generation (5G) communication system, which aims to provide connections to a very large number of Internet of Things (IoT) devices and facilitate sporadical transmission, e.g., [1], [2], [3]. These complicated scenarios inherent in mMTC often render the acquisition of channel state information (CSI) at the base station (BS) impractical, hampering the way in which massive connectivity could be achieved. Prominent techniques, such as massive multiple-input multiple-output (MIMO) [4], [5] or space division multiple access (SDMA) [6], non-orthogonal multiple access (NOMA) [7], and rate-splitting multiple access (RSMA) [8], have shown promises but under these circumstances, they may not be feasible options.

The work of K. K. Wong is supported by the Engineering and Physical Sciences Research Council (EPSRC) under Grant EP/W026813/1.

The work of H. Hong is supported by the Outstanding Doctoral Graduates Development Scholarship of Shanghai Jiao Tong University.

The work of R. Murch is supported by the Hong Kong Research Grants Council Area of Excellence grant AoE/E-601/22-R.

The work of Y. Xu and D. He is supported in part by National Natural Science Foundation of China under Grant 62271316 and 62422111.

H. Hong and K. K. Wong are with the Department of Electronic and Electrical Engineering, University College London, London, United Kingdom. K. K. Wong is also affiliated with the Department of Electronic Engineering, Kyung Hee University, Yongin-si, Gyeonggi-do 17104, Korea.

H. Xu is with the National Mobile Communications Research Laboratory, Southeast University, Nanjing 210096, China.

Y. Xu, D. He, and W. Zhang are with the Cooperative Medianet Innovation Center (CMIC), Shanghai Jiao Tong University, Shanghai, China.

H. Shin is with the Department of Electronic Engineering, Kyung Hee University, Yongin-si, Gyeonggi-do 17104, Korea.

R. Murch is with the Department of Electronic and Computer Engineering and Institute for Advanced Study (IAS), The Hong Kong University of Science and Technology, Clear Water Bay, Hong Kong SAR, China.

Corresponding author: Kai-Kit Wong.

To improve scalability, we need a straightforward multiple access scheme that allows for massive spectrum sharing and requires less transmitter CSI. A promising approach to tackle this challenge is fluid antenna multiple access (FAMA) [9]. FAMA takes great advantage of the antenna position flexibility enabled by the fluid antenna system (FAS) technology to operate at the natural interference null for reception [10].

The concept of FAS was proposed in 2020 by Wong *et al.* [11], [12]. Its implementation relies on flexible technologies that may be realized in the form of liquid-based antennas [13], [14], [15], reconfigurable pixel-based antennas [16], [17], stepper motor-based antennas [18], or flexible structures using metamaterials [19]. Recent studies in FAS have already investigated the performance in different channels [20], [21], [22], [23], [24], [25]. Some related results came under the name of movable antenna system (MAS) that could be regarded as a special case within the field of FAS [26].Channel estimation for FAS has also been studied recently recognizing the key role of spatial correlation [27], [28], [29].

Efforts have also been made to combine FAS with other technologies. For instance, combined with MIMO, FAS can optimize diversity-multiplexing trade-offs and q-outage capacity [30]. For integrated sensing and communication (ISAC), FAS balances sensing-communication trade-offs via reconfigurable beam alignment [31]. For full-duplex communication, FAS mitigates self-interference by spatially separating transceivers [32]. The integration of FAS and over-the-air computation reduces channel misalignment errors in distributed tasks [33], and FAS-aided reconfigurable intelligent surfaces (RIS) address mutual coupling to boost efficiency [34]. In multiuser uplink, FAS can enhance capacity by adjusting the positions and rotations based on user distribution [35], [36].

For downlink communications, FAMA was first introduced in 2022 [9]. It exploits the unique feature of FAS to access the spatial opportunity where the interference becomes weak. Depending on how fast the user updates the position (a.k.a. port) of FAS, FAMA can be classified into *fast* FAMA (*f*-FAMA) [9], [37] or *slow* FAMA (*s*-FAMA) [38], [39], [40], [41], [42], [43]. The *f*-FAMA scheme switches the antenna port on a per-symbol basis, where the data-dependant sum interference plus noise signal cancels. However, f-FAMA could be impractical because of the complexity of instantaneously observing a large number of received signals. By contrast, *s*-FAMA is a more practical scheme because it only requires the FAS to switch the position once during each channel coherence time. Recently in [44], [45], 5G New Radio (NR) coded modulation schemes have also been considered to improve FAMA.

Nonetheless, state-of-art researches on FAS and FAMA have been based on narrowband channels with flat fading characteristics. But in real channels, broadband communications is

more likely and the adoption of orthogonal frequency-division multiplexing (OFDM) is necessary to resolve the delay spread [46]. Technically speaking, there is concern if FAS could still perform well in OFDM settings because a desirable port at a subcarrier is likely not as desirable for other subcarriers. Recently, [47] has examined wideband FAS transmission with an emphasis on optimizing antenna positions, but it did not address the integration of FAS into the 5G NR settings. It is important to find out if FAS is indeed useful for 5G NR.

Motivated by the above, this paper integrates FAMA within the OFDM system, resulting in the proposed OFDM-FAMA system. This framework enables the BS to effectively distribute the signals to multiple user terminals (UTs) without requiring CSI at the BS or the need of interference cancellation at the UTs. Our effort aligns with the 5G NR physical layer procedures, and proposes a port selector along with an interference rejection combining (IRC) equalizer tailored for FAS. Besides, semi-analytical achievable rates are derived, and are then used to optimize the configuration of FAS. Importantly, we conduct link-level simulations to assess the block error rate (BLER) of the communication links of the OFDM-FAMA system.

Our main contributions are summarized as follows:

- First, we develop a framework for OFDM-FAMA, facilitating downlink FAMA within the 5G NR architecture. The transmitter adheres to the physical layer procedures of 5G NR [48], including channel coding [49] and OFDM modulation [50]. At the receiver side, we have developed a port selection mechanism for both training and running stages. Two distinct training strategies are proposed to switch the radio frequency (RF) chains among various fluid antenna ports during the training stage and identify those with the highest signal-to-interference plus noise ratio (SINR). Furthermore, an IRC equalizer is implemented to further mitigate the interference.
- Three metrics related to the achievable rates of OFDM-FAMA are derived: the average outage rate, the average mutual information (AMI), and the cutoff rate. Moreover, we propose an algorithm to approximate the suboptimal configuration for the FAS at each user, based on the semi-analytical achievable rate. Simulation results reveal that this suboptimal FAS configuration enables OFDM-FAMA to obtain near-optimal system performance.
- Finally, link-level simulations are conducted considering the tapped delay line (TDL) channel model from the 3rd Generation Partnership Project (3GPP) [51] to assess the physical layer performance of OFDM-FAMA. Comprehensive BLER results confirm the superior multiplexing gain offered by OFDM-FAMA, particularly in cases with robust channel coding and low spectrum efficiency.

Notations: Scalars are represented by lowercase letters while vectors and matrices are denoted by lowercase and uppercase boldface letters, respectively. Transpose and hermitian operations are denoted by superscript T and $\dagger$, respectively. Also, $\lceil\cdot\rceil$ and $\lfloor\cdot\rfloor$ are the ceiling and floor operation, respectively. For a complex scalar x, $|x|$ represents its modulus. The notation $*$ denotes the circular convolution operation.

II. Review of FAMA

Before we consider the OFDM-FAMA system, we briefly introduce the FAMA model. In FAMA, an interference channel with U UTs is considered. Each UT is equipped with an $N = (N_1 \times N_2)$-port two-dimensional FAS (2D-FAS) with a physical size of $W_1\lambda \times W_2\lambda$, where λ is the carrier wavelength. Over the 2D space, N_i ports are uniformly distributed along a linear space of length $W_i\lambda$ for $i \in \{1, 2\}$. For simplicity, we map the antenna port $(k_1, k_2) \to k : k = k_1 \times N_2 + k_2$, where $k_1 \in \{0, \ldots, N_1 - 1\}$, $k_2 \in \{0, \ldots, N_2 - 1\}$, and $k \in \{0, \ldots, N - 1\}$. The received signal at the k-th port of user u is modelled as

$$r_k^{(u)}[t] = g_k^{(u,u)} s^{(u)}[t] + \sum_{\substack{\tilde{u}=1 \\ \tilde{u}\neq u}}^{U} g_k^{(\tilde{u},u)} s^{(\tilde{u})}[t] + \eta_k^{(u)}[t], \tag{1}$$

where $g_k^{(\tilde{u},u)}$ is the fading channel from the $\tilde{u}$-th BS antenna to UT u at the k-th port, $\eta_k^{(u)}[t]$ is the zero-mean complex Gaussian noise with variance of σ_η^2, and $s^{(u)}[t]$ is the transmitted symbol for UT u with $\mathbb{E}[|s^{(u)}|^2] = 1$.

The channels $\{g_k^{(\tilde{u},u)}\}_{\forall k}$ are correlated. With the eigenvalue-based model in [20] and assuming rich scattering, the channel $g_k^{(\tilde{u},u)}$ can be expressed as

$$g_k^{(\tilde{u},u)} = \sigma^{(\tilde{u},u)} \sum_{l=1}^{N} \sqrt{\lambda_l}\mu_{k,l}\alpha_l, \tag{2}$$

where $\alpha_l \sim \mathcal{CN}(0, 1)$, λ_l and $\mu_{k,l}$ are obtained from the singular value decomposition (SVD) of the channel covariance matrix $\boldsymbol{\Sigma}$. For simplicity, we set $\sigma^{(\tilde{u},u)} = \sigma, \forall \tilde{u}, u$. In this case, the channel covariance matrix can be expressed as

$$\mathbb{E}\left[\boldsymbol{g}^{(\tilde{u},u)}\left(\boldsymbol{g}^{(\tilde{u},u)}\right)^{\dagger}\right] = \sigma^2\boldsymbol{\Sigma}, \tag{3}$$

where $\boldsymbol{g}^{(\tilde{u},u)} = [g_1^{(\tilde{u},u)}, \ldots, g_N^{(\tilde{u},u)}]^T$, and we have

$$[\boldsymbol{\Sigma}]_{k,l} = J_0\left(2\pi\sqrt{\left(\frac{k_1 - l_1}{N_1 - 1}W_1\right)^2 + \left(\frac{k_2 - l_2}{N_2 - 1}W_2\right)^2}\right), \tag{4}$$

where $(l_1, l_2) \to l$, and $J_0(\cdot)$ is the zero-order Bessel function of the first order. SVD is carried out as $\boldsymbol{\Sigma} = \boldsymbol{U}\boldsymbol{\Lambda}\boldsymbol{U}^{\dagger}$, where $\boldsymbol{\Lambda} = \mathrm{diag}(\lambda_1, \ldots, \lambda_N)$, and $[\boldsymbol{U}]_{k,l} = \mu_{k,l}$.

The key point of FAMA is to select the antenna port(s) with highest SINR at each user for multiple access, i.e.,

$$k_n^* = \arg \max_{k \setminus \{k_0^*, \ldots, k_{n-1}^*\}} \Gamma_k, \ n = 0, \ldots, N^* - 1, \tag{5}$$

where N^* denotes the number of the selectable antenna ports which depends on the number of RF chains, and Γ_k is the average SINR when considering s-FAMA [38]:

$$\Gamma_k^{s\text{-}FAMA} = \frac{|g_k^{(u,u)}|^2}{\sum_{\substack{\tilde{u}=1 \\ \tilde{u}\neq u}}^{U} |g_k^{(\tilde{u},u)}|^2 + \sigma_\eta^2}. \tag{6}$$

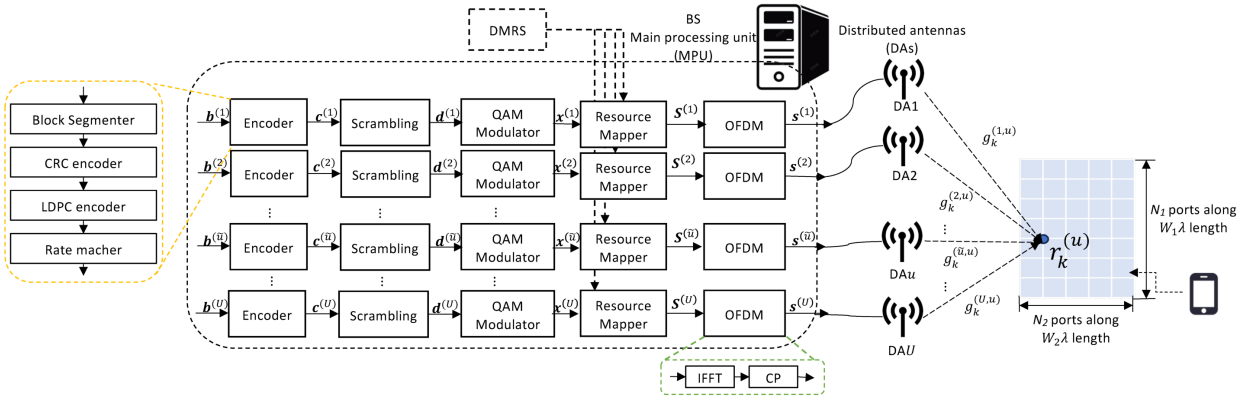

Fig. 1: System model of the downlink OFDM-FAMA system to a particular UT.

III. Downlink OFDM-FAMA

In this paper, we consider a downlink OFDM-FAMA system in which the BS communicates to U UTs, each equipped with a FAS. As illustrated in Fig. 1, the BS has a main processing unit (MPU) and U distributed antennas, each responsible for transmitting an information-bearing signal to one designated UT. This configuration enables each UT to utilize its FAS to select optimal spatial ports. By shifting the responsibility of interference management and channel optimization to the UT themselves, CSI is unnecessary at the BS. Additionally, the distributed antennas ensure that the transmission to each UT occurs independently. This decentralized design removes CSI feedback loops, minimizes latency and overhead, and enhances scalability in massive connectivity environments.

At the MPU, the information sequences of U users are processed in parallel with U layers using the same modulation coding scheme (MCS). At the u-th layer, the information bit sequence $\boldsymbol{b}^{(u)} = [b_0^{(u)}, \ldots, b_{N_a-1}^{(u)}]$ is encoded to bit sequence $\boldsymbol{c}^{(u)} = [c_0^{(u)}, \ldots, c_{N_b-1}^{(u)}]$, where N_a is equal to the transmit block size (TBS), $N_b = N_{\text{RE}} \times Q_m$ is the number of total transmitted data bits, N_{RE} is the number of resource elements (RE) for data transmission, and Q_m is the modulation order. A 5G NR encoder is considered, and the encoder includes the block segmenter, the cyclic redundancy check (CRC) encoder, the low-density parity-check (LDPC) encoder, and the rate matcher. The overall code rate can be expressed as

$$\text{CR} = N_a/N_b = \text{TBS}/(N_{\text{RE}} \times Q_m). \tag{7}$$

The encoded bit sequence $\boldsymbol{c}^{(u)}$ is scrambled by a user-specific scramble sequence to randomize the date pattern. The scrambled bit sequence $\boldsymbol{d}^{(u)} = [d_0^{(u)}, \ldots, d_{N_a-1}^{(u)}]$ is mapped to a symbol sequence $\boldsymbol{x}^{(u)} = [x^{(u)}[0], \ldots, x^{(u)}[N_s-1]]$, in which $N_s = N_b/Q_m = N_{\text{RE}}$. The bit interleaved coded modulation (BICM) efficiency calculating the coding modulation efficiency is thereby denoted as

$$E_{\text{BICM}} = \text{CR} \times Q_m = \text{TBS}/N_{\text{RE}} \text{ [bit/channel use]}. \tag{8}$$

The symbol sequence $\boldsymbol{x}^{(u)}$ is then mapped to the specific u-th antenna and the physical resource blocks (PRBs) for OFDM transmission. The symbol matrix $\boldsymbol{S}^{(u)}$ consists of $N_{\text{symb}}^{\text{subframe}} \times (N_{\text{PRB}} \cdot N_{\text{sc}}^{\text{RB}})$ symbols, including data symbols $\boldsymbol{x}^{(u)}$ and the demodulation reference signal (DMRS) symbols, where $N_{\text{symb}}^{\text{subframe}}$ represents the number of OFDM symbols per subframe, N_{PRB} is the number of PRBs, and $N_{\text{sc}}^{\text{RB}}$ is the number of subcarriers per resource block (RB). The symbol matrix $\boldsymbol{S}^{(u)}$ is then OFDM modulated as $\boldsymbol{s}^{(u)} = [s^{(u)}[0], \ldots, s^{(u)}[N_s^{\text{subframe}}-1]]$ and transmitted at the u-th distributed antenna, where $N_s^{\text{subframe}} = N_{\text{symb}}^{\text{subframe}} \cdot N_{\text{fft}} + N_{\text{CP}}$ is the total number of transmitted symbols per subframe in the time domain, N_{fft} is the fast Fourier transform (FFT) size, and N_{CP} is the length of the cyclic prefix (CP). Therefore, the overall spectrum efficiency (SE) is calculated as

$$\text{SE} = \text{TBS}/(T_{\text{subframe}} \times \text{BW}) \text{ [bit/s/Hz]}, \tag{9}$$

where $T_{\text{subframe}} = 1$ ms is the duration of a subframe and BW is the bandwidth.

The u-th UT's receiver with N_{RF} RF chains is depicted in Fig. 2, and the received signal at the k-th port in the time domain can be expressed as

$$r_k^{(u)}[t] = g_k^{(u,u)}[t] * s^{(u)}[t] + \sum_{\tilde{u} \neq u} g_k^{(\tilde{u},u)}[t] * s^{(\tilde{u})}[t] + \eta_k[t]. \tag{10}$$

We consider the 3GPP TDL channel model with the power and delay profile specified in [51, Clause 7.7.2]. Considering the highly correlated FAS ports, we apply the correlation matrix defined in (4) as the correlation parameter of the TDL channel [51, Clause 7.7.5.2], [52].

With OFDM demodulation, the received signal is transformed, and can be described in the frequency domain as

$$\begin{aligned} R_k[n,m] &= G_k^{(u,u)}[n,m] S^{(u)}[n,m] \\ &\quad + \sum_{\tilde{u} \neq u} G_k^{(\tilde{u},u)}[n,m] S^{(\tilde{u})}[n,m] + Z_k[n,m], \end{aligned} \tag{11}$$

where $R_k[n,m]$ is the m-th FFT bin of the n-th OFDM symbol in the received grid $\boldsymbol{R}_k$, $n = 0, \ldots, N_{\text{symb}}^{\text{subframe}} - 1$, $m = 0, \ldots, N_{\text{PRB}} \cdot N_{\text{sc}}^{\text{RB}} - 1$. Similarly, $G_k^{(\tilde{u},u)}[n,m]$, $S^{(\tilde{u})}[n,m]$, and $Z_k[n,m]$ are the (n,m)-th elements in the channel grid $\boldsymbol{G}_k^{(\tilde{u},u)}$, the transmitted symbol grid $\boldsymbol{S}^{(\tilde{u})}$, and the Gaussian

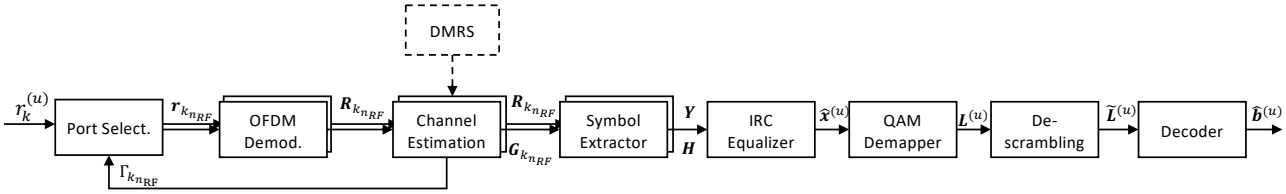

Fig. 2: Receiving block diagram of the u-th UT.

noise grid $\boldsymbol{Z}_k$, respectively. With FFT operation, these frequency domain signals are given by

$$R_k[n,m] = \text{FFT}(r_k[t], N_{\text{fft}}), \tag{12}$$
$$G_k^{(\tilde{u},u)}[n,m] = \text{FFT}(g_k^{(\tilde{u},u)}[t], N_{\text{fft}}), \tag{13}$$
$$S^{(\tilde{u})}[n,m] = \text{FFT}(s^{(\tilde{u})}[t], N_{\text{fft}}), \tag{14}$$
$$Z_k[n,m] = \text{FFT}(\eta_k[t], N_{\text{fft}}). \tag{15}$$

For FAMA, each UT needs to switch to the best port(s) with the highest SINR(s) [9]. As shown in Fig. 2, in the OFDM-FAMA system, the average SINR is measured in the frequency domain subframe-by-subframe after channel estimation, while the port selection based on the SINR should be processed in the time domain.[1] Hence, the measured subframe-average SINRs of antenna ports are fed back to the port selection block, and a mapping between the RF chains and the fluid antenna ports, $(n_{\text{RF}} \to k) : \{k_{n_{\text{RF}}}\}$, $n_{\text{RF}} = 0, \ldots, N_{\text{RF}} - 1$, is obtained from the measured SINR. But the SINR is incomplete at the beginning of the reception, so we divide the receiving process into training and running stages as shown in Fig. 3.

During the training stage, the RF chains are switched among the fluid antenna ports subframe by subframe to measure the SINRs of the fluid antenna ports, and the mapping $\{k_{n_{\text{RF}}}^{(n_{\text{subframe}})}\}$ is obtained from the training strategy. In the running stage, the mapping $\{k_{n_{\text{RF}}}^*\}$ depends upon SINR ordering, in which the antenna ports with the highest SINR are chosen as the active ports. It is worth noting that during the training stage, the data transmission is not interrupted but is transmitted at a relatively lower transmission rate. Meanwhile, the SINR of the selected ports is measured during the running stage, and the system will switch back to the training stage if the SINR changes. Note that the switching frequency is affected by the coherence time of the channel, which exhibits an inverse relationship with the Doppler frequency. In high mobility situations, the switching frequency will increase. The details of the FAS port selection and training strategies will be explained in Section III-A.

For the n_{RF}-th RF chain at a UT receiver, assuming perfect timing synchronization, the received signal at the $k_{n_{\text{RF}}}$-th port $\boldsymbol{r}_{k_{n_{\text{RF}}}} = [r_{k_{n_{\text{RF}}}}[0], \ldots, r_{k_{n_{\text{RF}}}}[N_s^{\text{subframe}} - 1]]$ is OFDM demodulated as the received grid $\boldsymbol{R}_{k_{n_{\text{RF}}}}$. Using the reference signal, the channel grid can be estimated as $\boldsymbol{G}_{k_{n_{\text{RF}}}}^{(u,u)}$. The data symbols and their channel are extracted from the received grid and the channel grid as $\boldsymbol{y}_{k_{n_{\text{RF}}}} = [y_{k_{n_{\text{RF}}}}[0], \ldots, y_{k_{n_{\text{RF}}}}[N_s - 1]]$ and $\boldsymbol{h}_{k_{n_{\text{RF}}}}^{(u,u)} = [h_{k_{n_{\text{RF}}}}^{(u,u)}[0], \ldots, h_{k_{n_{\text{RF}}}}^{(u,u)}[N_s - 1]]$, respectively. From

[1]In the frequency domain, it would be difficult to come up with a metric that can select the proper port affecting multiple subcarriers.

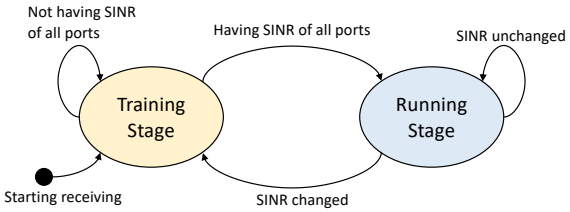

Fig. 3: Stage chart of the receiver.

(11), the relationship between the extracted data symbol and the channel can be expressed as

$$y_{k_{n_{\text{RF}}}}[l] = h_{k_{n_{\text{RF}}}}^{(u,u)}[l] \cdot x^{(u)}[l] + \eta_{k_{n_{\text{RF}}}}^{\text{I}}[l], \tag{16}$$

where the interference and noise signal is given by

$$\eta_{k_{n_{\text{RF}}}}^{\text{I}}[l] = \sum_{\tilde{u} \neq u} h_{k_{n_{\text{RF}}}}^{(\tilde{u},u)}[l] \cdot x^{(\tilde{u})}[l] + \eta[l], \tag{17}$$

where $\{h_{k_{n_{\text{RF}}}}^{(\tilde{u},u)}\}$ is the channel coefficient from the $\tilde{u}$-th antenna at the BS to the $k_{n_{\text{RF}}}$-th port selected by the n_{RF}-th RF chain of the u-th UT which is unknown at the u-th UT, and $\eta[l]$ is the complex Gaussian noise with variance of σ_η^2.

Combining all N_{RF} RF chains, the received symbol matrix can be expressed as $\boldsymbol{Y} = [\boldsymbol{y}_{k_0}^T, \ldots, \boldsymbol{y}_{k_{N_{\text{RF}}-1}}^T]^T$, while the channel matrix is $\boldsymbol{H} = [\boldsymbol{h}_{k_0}^{(u,u)^T}, \ldots, \boldsymbol{h}_{k_{N_{\text{RF}}-1}}^{(u,u)^T}]^T$. With the IRC equalization, we can have the equalized symbol sequence $\hat{\boldsymbol{x}}^{(u)} = [\hat{x}^{(u)}[0], \ldots, \hat{x}^{(u)}[N_s - 1]]$. This IRC equalization will be fully introduced in Section III-B. The soft demapper is then adopted to have the log-likelihood ratio (LLR) sequence $\boldsymbol{L}^{(u)} = [L_0^{(u)}, \ldots, L_{N_b-1}^{(u)}]$, and this LLR sequence is descrambled and decoded to restore the information bit sequence.

A. Port Selection and Training Strategy

In the port selection process, N_{RF} fluid antenna ports with the highest average SINRs are supposed to receive the signals, but this can be realized only in the running stage after the SINRs of all ports have been fully acknowledged. When the receiver does not yet know the SINRs of all ports (e.g., at the beginning of the reception), the RF chains should be switched among the fluid antenna ports on a subframe basis to measure the SINRs during reception. This phase is referred to as the training stage. The number of subframes for the training stage, $N_{\text{subframe}}^{\text{TS}}$, is determined by the number of ports N, the number of RF chains N_{RF}, and the training strategies employed.

In this paper, we propose two training strategies for the RF chains to switch amongst the antenna ports and measure

Algorithm 1 Training Strategy A for Port Selection

Require: N, N_{RF};
Ensure: Training stage $\{k_{n_{\mathrm{RF}}}^{(n_{\mathrm{subframe}})}\}$, Running stage $\{k_{n_{\mathrm{RF}}}^{*}\}$;
Interleave the antenna ports as (18);
for $n_{\mathrm{subframe}} = 0$ to $N_{\mathrm{subframe}}^{\mathrm{TS}A} - 1$ **do**
  for $n_{\mathrm{RF}} = 0$ to $N_{\mathrm{RF}} - 1$ **do**
    $k_{n_{\mathrm{RF}}}^{(n_{\mathrm{subframe}})} = \kappa_{(n_{\mathrm{subframe}} \times N_{\mathrm{RF}} + n_{\mathrm{RF}}) \mod N}$;
  end for
  Switch the RF chains to the $\{k_{n_{\mathrm{RF}}}^{(n_{\mathrm{subframe}})}\}$-th fluid antenna ports;
  Measure the SINR of the $\{k_{n_{\mathrm{RF}}}^{(n_{\mathrm{subframe}})}\}$-th fluid antenna ports: $\{\Gamma_{k_{n_{\mathrm{RF}}}^{(n_{\mathrm{subframe}})}}\}$;
end for
Sort the SINR list $\mathbf{\Gamma} = \{\Gamma_0, \dots \Gamma_{N-1}\}$;
Select N_{RF} ports with largest SINR $\{k_{n_{\mathrm{RF}}}^{*}\}$ as (5).

Algorithm 2 Training Strategy B for Port Selection

Require: N, N_{RF};
Ensure: Training stage $\{k_{n_{\mathrm{RF}}}^{(n_{\mathrm{subframe}})}\}$, Running stage $\{k_{n_{\mathrm{RF}}}^{*}\}$;
$\Gamma_k = -\inf, \forall k \in \{0, \dots, N-1\}$;
Interleave the antenna ports as (18);
for $n_{\mathrm{subframe}} = 0$ to $N_{\mathrm{subframe}}^{\mathrm{TS}B} - 1$ **do**
  for $n_{\mathrm{RF}} = 0$ to $\lfloor N_{\mathrm{RF}}/2 \rfloor - 1$ **do**
    $k_{n_{\mathrm{RF}}}^{(n_{\mathrm{subframe}})} = \kappa_{[(n_{\mathrm{subframe}}+1) \times \lfloor N_{\mathrm{RF}}/2 \rfloor + n_{\mathrm{RF}}] \mod N}$;
  end for
  for $n_{\mathrm{RF}} = \lfloor N_{\mathrm{RF}}/2 \rfloor$ to $N_{\mathrm{RF}} - 1$ **do**
    if $n_{\mathrm{subframe}} = 0$ **then**
      $k_{n_{\mathrm{RF}}}^{(n_{\mathrm{subframe}})} = \kappa_{n_{\mathrm{RF}} - \lfloor N_{\mathrm{RF}}/2 \rfloor}$;
    else
      $k_{n_{\mathrm{RF}}}^{(n_{\mathrm{subframe}})} = \arg \max_{k \setminus \{k_{\lfloor N_{\mathrm{RF}}/2 \rfloor}^{(n_{\mathrm{subframe}})}, \dots, k_{n_{\mathrm{RF}}-1}^{(n_{\mathrm{subframe}})}\}} \Gamma_k$;
    end if
  end for
  Switch to the $\{k_{n_{\mathrm{RF}}}^{(n_{\mathrm{subframe}})}\}$-th fluid antenna ports;
  Measure the SINR: $\{\Gamma_{k_{n_{\mathrm{RF}}}^{(n_{\mathrm{subframe}})}}\}$;
end for
Sort the SINR list $\mathbf{\Gamma} = \{\Gamma_1, \dots \Gamma_N\}$;
Select N_{RF} ports with largest SINR $\{k_{n_{\mathrm{RF}}}^{*}\}$ as (5).

the SINRs. *Strategy A* switches all the RF chains, while *Strategy B* switches half of the RF chains and selects the other half from the ports with known SINRs. These two training strategies are described in Algorithms 1 and 2, respectively. The algorithms define the port mapping $\{k_{n_{\mathrm{RF}}}^{(n_{\mathrm{subframe}})}\}$ for the n_{subframe}-th subframe during the training stage, and determine the optimal FAS port mapping $\{k_{n_{\mathrm{RF}}}^{*}\}$ of the running stage after obtaining knowledge of all the ports' SINRs.

During training, the antenna port will first be interleaved to minimize correlation between the selected antenna ports. The k-th port is interleaved to the κ_k-th port with an interval Δ as

$$\kappa_k = \begin{cases} \Delta s + t, & \text{if } k < \Delta \lfloor N/\Delta \rfloor,\ k = \Delta t + s, \\ & t = 0, 1, \dots, \lfloor N/\Delta \rfloor - 1, \\ & s = 0, 1, \dots, \Delta - 1, \\ k, & \text{if } k \geq \Delta \lfloor N/\Delta \rfloor, \end{cases} \tag{18}$$

where the interval $\Delta = \lceil N/N_{\mathrm{RF}} \rceil$ for *Strategy A*, and $\Delta = \lceil N/\lfloor N_{\mathrm{RF}}/2 \rfloor \rceil$ for *Strategy B*. From the 0-th to the $(N_{\mathrm{subframe}}^{\mathrm{TS}} - 1)$-th subframe, the RF chains switch among the fluid antenna ports to measure the SINR, $\{\Gamma_{k_{n_{\mathrm{RF}}}^{(n_{\mathrm{subframe}})}}\}$. The total number of subframes for training in *Strategy A* is given by

$$N_{\mathrm{subframe}}^{\mathrm{TS}A} = \lceil N/N_{\mathrm{RF}} \rceil, \tag{19}$$

whereas $N_{\mathrm{subframe}}^{\mathrm{TS}}$ for *Strategy B* is given by

$$N_{\mathrm{subframe}}^{\mathrm{TS}B} = \lceil (N - \lceil N_{\mathrm{RF}}/2 \rceil)/\lfloor N_{\mathrm{RF}}/2 \rfloor \rceil. \tag{20}$$

Comparing these two numbers, it is evident that *Strategy A* uses fewer subframes during the training stage. After exploring all the fluid antenna ports in the training stage, the subframe basis average SINR list $\mathbf{\Gamma} = \{\Gamma_0, \dots, \Gamma_{N-1}\}$ is established as the basis for port selection. The optimal port mapping for the running stage can be determined using the FAMA port selection method in (5) by sorting the average SINR list $\mathbf{\Gamma}$.

The data transmission performance of the training stage is expected to be lower than that during the running stage. This is because the RF chains may switch to those fluid antenna ports with relatively low SINRs. As a result, the performance of *Strategy B* could surpass that of *Strategy A* after several subframes of training, as *Strategy B* dynamically adjusts the RF chains during the training stage. This will be demonstrated by the link-level simulations in Section V-D.

In general, there exists a trade-off between the number of training subframes (i.e., the training time) and the data rate during the training stage. Specifically, *Strategy A* employs fewer subframes while sustaining a low transmission rate throughout the training stage. In contrast, *Strategy B* utilizes approximately double the number of subframes, but the transmission rate increases during the training stage. The selection between these two strategies should be based on practical implementation considerations.

B. IRC Equalization

The extracted received symbols among the N_{RF} RF chains $\boldsymbol{Y} = [\boldsymbol{y}[0], \dots, \boldsymbol{y}[N_s - 1]]$ are combined at the IRC equalizer, where $\boldsymbol{y}[l]$ is the l-th column of $\boldsymbol{Y}$. The minimum mean-square-error (MMSE) equalized vector for the m-th received symbol $\boldsymbol{y}[l] = [y_{k_0}[l], \dots, y_{k_{N_{\mathrm{RF}}-1}}[l]]^T$ is given by

$$\boldsymbol{w}[l] = \boldsymbol{h}^{\dagger}[l](\boldsymbol{h}[l]\boldsymbol{h}^{\dagger}[l] + \hat{\mathbf{\Sigma}})^{-1}, \tag{21}$$

where $\boldsymbol{h}[l] = [h_{k_0}^{(u,u)}[l], \dots, h_{k_{N_{\mathrm{RF}}-1}}^{(u,u)}[l]]^T$ is the channel vector and the l-th column vector of the channel matrix $\boldsymbol{H}$, $\hat{\mathbf{\Sigma}}$ is the estimated covariance matrix of the interference and noise $\boldsymbol{\eta}^{\mathrm{I}}[l] = [\eta_{k_0}^{\mathrm{I}}[l], \dots, \eta_{k_{N_{\mathrm{RF}}-1}}^{\mathrm{I}}[l]]^T$. The covariance matrix can be easily estimated as $\hat{\mathbf{\Sigma}} = [(U-1)\sigma^2\mathbf{\Sigma} + \sigma_\eta^2 \boldsymbol{I}]_{\{k_{n_{\mathrm{RF}}}\}}$ [44], or dynamically estimated from the reference signal (RS) as [53]

$$\hat{\mathbf{\Sigma}} = \frac{1}{N_{\mathrm{RS}}} \sum_{l=0}^{N_{\mathrm{RS}}} (\boldsymbol{y}_{\mathrm{RS}}[l] - \boldsymbol{h}_{\mathrm{RS}}[l] x_{\mathrm{RS}}^{(u)}[l]) \times (\boldsymbol{y}_{\mathrm{RS}}[l] - \boldsymbol{h}_{\mathrm{RS}}[l] x_{\mathrm{RS}}^{(u)}[l])^{\dagger}, \tag{22}$$

in which N_{RS} denotes the number of RS elements, $x_{\mathrm{RS}}^{(u)}$ is the RS transmitted symbol, $\boldsymbol{y}_{\mathrm{RS}}$ and $\boldsymbol{h}_{\mathrm{RS}}$ are the RS received

vector and the channel vector extracted from the received grids $\{\boldsymbol{R}_k\}$ and the channel grids $\{\boldsymbol{G}_k^{(u,u)}\}$, respectively. The fixed estimation is simpler, while the dynamical estimation can be more accurate with a sufficiently long RS.

The equalized symbol thus can be expressed as

$$\begin{aligned}\hat{x}^{(u)}[l] &= \beta \boldsymbol{w}[l]\boldsymbol{y}[l] \\ &= \beta \boldsymbol{w}[l]\boldsymbol{h}[l]x^{u}[l] + \beta \boldsymbol{w}[l]\boldsymbol{\eta}^{\mathrm{I}}[l],\end{aligned} \tag{23}$$

where $\beta = \sqrt{1/\mathbb{E}_l\{|\boldsymbol{w}[l]\boldsymbol{h}[l]|\}}$ is the normalized factor.

In the equalized symbol (23), $\beta \boldsymbol{w}\boldsymbol{h}x^{(u)}$ is the desired signal part, while $\beta \boldsymbol{w}\boldsymbol{\eta}^{\mathrm{I}}$ is the noise and interference part. Thus, the average SINR $\overline{\Gamma}$ of the subframe is given by

$$\begin{aligned}\overline{\Gamma} &= \frac{\mathbb{E}_l\left\{|\beta \boldsymbol{w}[l]\boldsymbol{h}[l]x^{(u)}[l]|^2\right\}}{\mathbb{E}_l\left\{|\beta \boldsymbol{w}[l]\boldsymbol{\eta}^{\mathrm{I}}[l]|^2\right\}} \\ &= 1/\mathbb{E}_l\left\{|\beta \boldsymbol{w}[l]\boldsymbol{\eta}^{\mathrm{I}}[l]|^2\right\}.\end{aligned} \tag{24}$$

This average SINR is the metric for performance evaluation.

C. Achievable Rate and FAS Configuration

The outage probability is defined as the occurrence of the average SINR $\overline{\Gamma}$ being less than the target SINR Γ. In other words, the outage probability for the u-th UT is given by

$$p_{\text{out}} \triangleq \text{Prob}\left(\overline{\Gamma} = \mathbb{E}\left\{1/|\beta \boldsymbol{w}[l]\boldsymbol{\eta}^{\mathrm{I}}[l]|^2\right\} < \Gamma\right). \tag{25}$$

For a specific MCS with BICM efficiency in (8), the target SINR for outage probability evaluation can be estimated as

$$\Gamma = 2^{\mathrm{TBS}/N_{\mathrm{RE}}} - 1. \tag{26}$$

The average outage rate can be evaluated by

$$C_\Gamma = U(1 - \text{Prob}(\overline{\Gamma} < \Gamma)) \times \frac{\mathrm{TBS}}{N_{\mathrm{RE}}}. \tag{27}$$

This corresponds to the case in which the BS transmits a fixed MCS with TBS information bits to the users. The multiplexing gain, M, is the capacity scaling factor given by

$$M = \frac{C_\Gamma}{\log_2(1+\Gamma)} = U(1 - \text{Prob}(\overline{\Gamma} < \Gamma)). \tag{28}$$

In addition to the outage rate in (27), the system rate can also be assessed through the AMI and the cutoff rate. The AMI per UT of OFDM-FAMA can be calculated as

$$C_B = Q_m + \sum_{i=1}^{Q_m} \mathbb{E}_{b,\boldsymbol{y},\boldsymbol{h}}\left[\log_2 \frac{\sum_{x\in\boldsymbol{\chi}_i^{(b)}} p_{\boldsymbol{h}}(\boldsymbol{y}|x)}{\sum_{x\in\boldsymbol{\chi}} p_{\boldsymbol{h}}(\boldsymbol{y}|x)}\right], \tag{29}$$

where the PDF $p(\boldsymbol{y}|x)$ is given by IRC as

$$p_{\boldsymbol{h}}(\boldsymbol{y}|x) = \frac{1}{\pi^{N_{\mathrm{RF}}}|\hat{\boldsymbol{\Sigma}}|}\exp\left[-(\boldsymbol{y}-\boldsymbol{h}x)^{\dagger}\hat{\boldsymbol{\Sigma}}^{-1}(\boldsymbol{y}-\boldsymbol{h}x)\right]. \tag{30}$$

Also, the cutoff rate can be obtained from the Bhattacharyya bound on the average bit-error probability in the absence of coding. The average Bhattacharyya factor is given by

$$B = \frac{1}{Q_m}\sum_{i=1}^{Q_m} \mathbb{E}_{b,\boldsymbol{y},\boldsymbol{h}}\left[\sqrt{\frac{\sum_{z\in(\chi)_i^{(\bar{b})}} p_{\boldsymbol{h}}(\boldsymbol{y}|x)}{\sum_{z\in(\chi)_i^{(b)}} p_{\boldsymbol{h}}(\boldsymbol{y}|x)}}\right]. \tag{31}$$

With that, the cutoff rate C_R can be written as

$$C_R = Q_m(1 - \log_2(B+1)). \tag{32}$$

Algorithm 3 Approximating FAS configuration N^*

Require: W, N_{RF}, U, threshold ϵ_C, ($\boldsymbol{\chi}$ or Γ)
Ensure: N^*
  $N_1 = N_2 = \lfloor\sqrt{N_{\mathrm{RF}}}\rfloor$; $C^{\lfloor\sqrt{N_{\mathrm{RF}}}\rfloor\times\lfloor\sqrt{N_{\mathrm{RF}}}\rfloor} = 0$;
  while $C^{(N_1\times N_2)} - C^{(N_1-1)\times(N_2-1)} > \epsilon_C$ **do**
    $N_1 = N_1 + 1$;
    $N_2 = N_2 + 1$;
    Calculate $C^{(N_1\times N_2)}$ for $N = N_1 \times N_2$;
  end while
  $N^* = N_1 \times N_2$;

In summary, the cutoff rate C_C ensures that channel codes are robust enough to handle channel variations, while BICM capacity C_B and average outage rate C_Γ set achievable rate targets under ergodic and non-ergodic conditions, respectively.

Now let us discuss the configuration of the FAS equipped at the UTs. Research in [20], [25] indicates that for a fixed FAS physical size $W = [W_1, W_2]$, the achievable rate may remain similar beyond a certain threshold N^*. Further, [25] proposed a method to approximate N^* for a given size W by analyzing the eigenvalues $\{\lambda_n\}$ of the channel covariance matrix $\boldsymbol{\Sigma}$. While this method is proven useful for FAS transmission with 1D-FAS, how the result can be extended to our OFDM-FAMA network utilizing the 2D-FAS at the receiver is unknown.

To address this, we present Algorithm 3 that approximates the suboptimal configuration N^* by directly evaluating the rate. For simplicity, a symmetrical 2D-FAS is considered, i.e., $W_1 = W_2$ and $N_1 = N_2$. The achievable rate $C^{(N_1\times N_2)}$ in Algorithm 3 can refer to the outage rate in (27), the AMI in (29), or the cutoff rate in (32). This algorithm determines the suboptimal N^* where OFDM-FAMA provides only a marginal improvement in the rate when $N > N^*$, given a threshold ϵ_C. Other system configurations, including the normalized physical size $W = [W_1, W_2]$, the number of supported UTs U, and the number of RF chains N_{RF}, need to be specified in the algorithm to calculate the achievable rate. If the AMI or cutoff rate is chosen as the metric, the modulation constellation $\boldsymbol{\chi}$ should be specified. If the outage rate is chosen as the criterion, the suboptimal N^* will depend on the target SINR Γ.

The complexity of the proposed method is greater than that of the approach in [25], since it employs Monte-Carlo numerical integration to calculate the achievable rates. Specifically, the computational complexity of calculating the rate $C^{(N_1\times N_2)}$ in each iteration of Algorithm 3 is $\mathcal{O}(N_M \times N_{\mathrm{RF}}^3)$ when employing the average outage rate and $\mathcal{O}(N_M \times Q_m \times N_{\mathrm{RF}}^2)$ when utilizing AMI or cutoff rate. In terms of the complexity, denote N_M as the number of channel realizations involved in the Monte-Carlo numerical integration process. Then the computational complexity of the average outage calculation is primarily dictated by the inverse operation during equalization (21) to calculate the average SINR. The complexity of AMI and cutoff rate calculations depends on the number of multiplication operations in PDF calculation in (30). Nevertheless, this algorithm is a one-time task. Therefore, its complexity does not adversely affect the overall process of OFDM-FAMA transmission, making this high complexity acceptable.

TABLE I: Simulation parameters.

Parameter	Value
Normalized size of FAS $[W_1, W_2]$	$[2,2]$, $[5,5]$
Number of ports $N_1 \times N_2$	From 2×2 to 15×15
Number of RF chains N_{RF}	2, 4, 16
Bandwidth	1.4 MHz
Number of PRBs N_{PRB}	6
Number of subcarriers per RB $N_{\text{sc}}^{\text{RB}}$	12
Subcarrier spacing Δf	15 kHz
Symbol duration	66.7 μs
CP duration	4.7 μs
FFT Size N_{fft}	128
Number of symbols per subframe $N_{\text{symb}}^{\text{subframe}}$	14
Number of resource elements N_{RE}	936
Signal-to-noise ratio (SNR) σ^2/σ_η^2	35 dB
Modulation coding scheme	MCSs in [48, Table 5.1.3.1-1]
Channel model	Block fading channel, TDL-C channel [51]
Delay spread $\text{DS}_{\text{desired}}$	30 ns
Maximum Doppler frequency	0, 30, 300 Hz

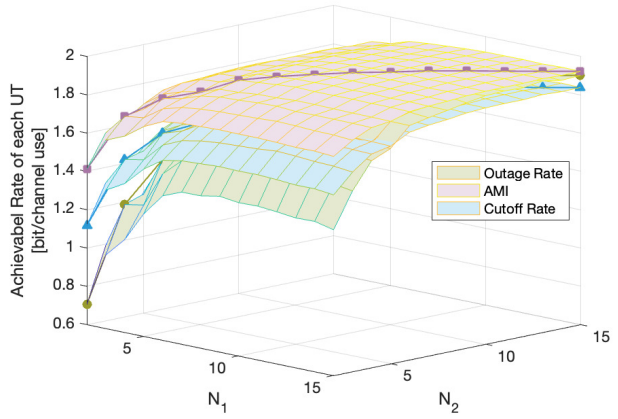

Fig. 4: Achievable rates of each UT with target SINR $\Gamma = 5$ dB, when $W = [2,2]$, $N_{\text{RF}} = 4$, and $U = 6$.

IV. Semi-Analytical Performance Evaluation

This section presents semi-analytical results to predict the performance of OFDM-FAMA during the running stage. Given the mathematical difficulties, Monte-Carlo simulations with $10,000$ independent channel realizations are used to compute these metrics. The analysis is conducted under the assumption of a rich scattering block fading channel with perfect channel estimation. As the evaluations pertain specifically to the running stage, we assume that the FAS at the UT is capable of identifying the ports with the highest average SINRs. Table I outlines the parameters and corresponding values considered in the evaluations. The carrier frequency is set as 5 GHz, resulting in a wavelength of $\lambda = 6$ cm. The normalized antenna sizes are W of $[2,2]$ and $[5,5]$, leading to the actual physical dimensions of 12 cm $\times$ 12 cm, and 30 cm $\times$ 30 cm, respectively.

A. Achievable Rate

Fig. 4 presents the results of the outage rate C_Γ, the mutual information C_B, and the cutoff rate C_R, against the 2D number of ports, N_1 and N_2, in the FAS-equipped UT in OFDM-FAMA, with $U = 6$ users. The physical size of FAS equipped at the UT is $2\lambda \times 2\lambda$. The modulation constellation utilized for evaluation of AMI and cutoff rate is quadrature phase shift keying (QPSK). For fair comparison, an uncoded QPSK system with target SINR of $\Gamma = 5$ dB is considered in the outage evaluation. The results indicate that the performance is symmetric. Consequently, we will maintain the symmetry condition (i.e., $N_1 = N_2$ and $W_1 = W_2$) throughout the rest of the simulations. In addition, an increase in the number of ports correlates with an enhancement in achievable rates, with a notable improvement observed when N is small, while the enhancement becomes marginal with large N.

With $N_1 = N_2$, different rate results against a range of parameters are shown in Fig. 5. The modulation constellation and the target SINR are the same as that in Fig. 4. Figs. 5(a)–5(c) consider the case when $N_{\text{RF}} = 4$, whereas Figs. 5(d)–5(f) pertain to $N_{\text{RF}} = 16$. When $N_{\text{RF}} = 4$ and $U = 4$, the rate is limited by the modulation order $Q_m = 2$ bit/channel use, or the Shannon capacity of target SINR Γ, calculated as $\log_2(1+\Gamma) = 2.06$ bit/channel use. In this case, error-free transmission is achievable, even when $N = 2 \times 2$, which degrades the antenna configuration at each UT to a fixed-position antenna (FPA). In addition, we can observe that the achievable rates become saturated when $N_{\text{RF}} = 16$ and $U = 15$, allowing for error-free transmission even under FPA condition ($N = 4 \times 4$). As the number of UTs U increases, the achievable rates have a positive correlation with the number of ports, $N = N_1 \times N_2$. The increasing of the rates is significant when N is small, but becomes marginal when N grows large. Note that the antenna port spacing is equal to $W_i\lambda/(N_i - 1)$, where $i \in 1, 2$. The saturation occurs when the antenna port spacing is relatively small, which results in a high correlation among the ports. Moreover, the number of ports N_1 or N_2 to ensure half-wavelength port spacing is indicated in Fig. 5(a), and the port spacing is smaller than $\lambda/2$ for the (N_1 or N_2) larger than the indicated point. It can be seen that the antenna port spacing at the point of saturation is always lower than $\lambda/2$, indicating that the design criterion of half-wavelength port spacing may not be applicable to FAS. A discussion regarding the suboptimal FAS configuration is provided in Section IV-B. The saturated rate for the system accommodating a large number of users ($U = 6$ or 8 for $N_{\text{RF}} = 4$ and $U = 20$ or 30 for $N_{\text{RF}} = 16$) is lower than 2 bit/channel use. Furthermore, when $N_{\text{RF}} = 16$ and $W = [2,2]$, the increasing of the achievable rate is marginal at the beginning, since the FPA with $N = 4 \times 4$ almost reaches the correlation saturation point over this physical size.

Note that when $N_{\text{RF}} = 16$ and $U = 30$, the outage rate nears 0 bit/channel use. The reason is that uncoded QPSK struggles to transmit signals for such a high number of users, underscoring the necessity for robust channel coding to support massive UTs. An intriguing observation is that when the number of antenna ports is exceedingly large, the achievable rate will slightly decrease with the increase of N_1 (or N_2), because of the correlation among the ports. This suggests that an excessive increase in the number of ports might adversely affect the overall performance.

Rate comparison with different physical sizes W indicates that a larger size of FAS at the UTs contributes to a higher achievable rate, with the disparity widening as the number

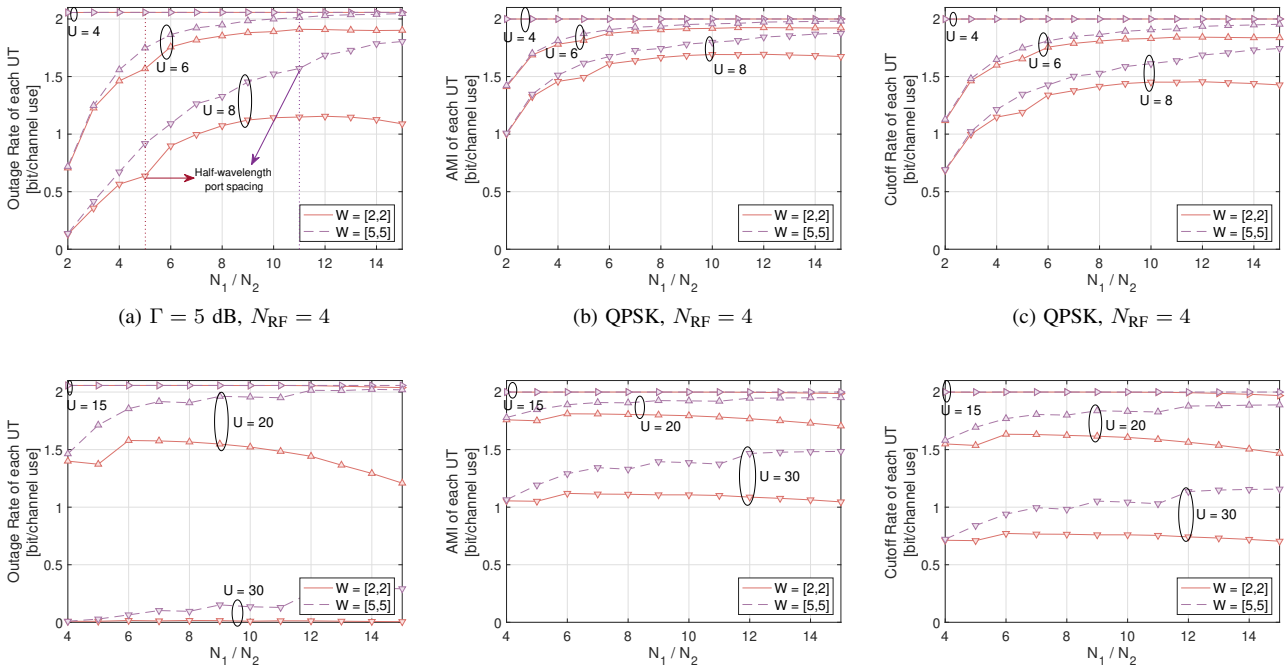

(a) $\Gamma = 5$ dB, $N_{\text{RF}} = 4$ (b) QPSK, $N_{\text{RF}} = 4$ (c) QPSK, $N_{\text{RF}} = 4$

(d) $\Gamma = 5$ dB, $N_{\text{RF}} = 16$ (e) QPSK, $N_{\text{RF}} = 16$ (f) QPSK, $N_{\text{RF}} = 16$

Fig. 5: Achievable rates of each UT against N_1 (or N_2), with different N_{RF}, W, and U, and the target SINR $\Gamma = 5$ dB.

TABLE II: Suboptimal N^* by Algorithm 3 for W and N_{RF} with different $C^{(N_1 \times N_2)}$, where $\epsilon_C = 0.02$ bit/channel use.

W	N_{RF}	U	criterion $C^{(N_1 \times N_2)}$			Algorithm 1 in [25]
			C_Γ	C_B	C_R	
$[2,2]$	4	6	9×9	7×7	7×7	5×5
		8	9×9	8×8	8×8	
	16	20	6×6	6×6	6×6	
		30	–	6×6	6×6	
$[5,5]$	4	6	9×9	7×7	7×7	8×8
		8	14×14	12×12	12×12	
	16	20	12×12	6×6	12×12	
		30	12×12	12×12	12×12	

of ports increases, because the saturated N^* is smaller for a small size W. On the other hand, the achievable rates of the system with FPA remain consistent when $W = [2,2]$ and $[5,5]$, which means the physical size does not significantly influence the performance of the system employing FPA, while it does affect the performance of OFDM-FAMA utilizing FAS.

B. Suboptimal FAS Configuration

Based on the rates in Fig. 5, we employ Algorithm 3 to find the suboptimal N^* for FAS at each UT with different W and N_{RF}. The threshold for the rate ϵ_C is set as 0.02 bit/channel use. With the exception of certain abrupt saturation instances, the suboptimal N^* for various configurations are demonstrated in Table II. The calculation is not performed when $C^{(N_1 \times N_2)} = C_\Gamma$, $W = [2,2]$, $N_{\text{RF}} = 16$, and $U = 30$, as the outage rate remains nearly zero in this case. Furthermore, the approximation results of [25, Algorithm 1] are included in the table for comparison. Given that [25, Algorithm 1] is specifically designed for 1D-FAS, we regard the $\lceil \sqrt{N_\lambda^*} \times \sqrt{N_\lambda^*} \rceil$ as the suboptimal solution for 2D-FAS at each UT, where N_λ^* is the suboptimal number of ports obtained from [25, Algorithm 1]. As shown in Table II and Fig. 5, the achievable rates at each UT of the OFDM-FAMA system demonstrate considerable improvements when N exceeds the suboptimal solution of [25, Algorithm 1]. Thus, it is wise to consider the pragmatic achievable rates during the design phase of the FAS configuration in the OFDM-FAMA system, despite the additional complexity.

C. Multiplexing Gain

The multiplexing gains of OFDM-FAMA are illustrated in Fig. 6, relative to the BICM efficiency of each UT, with the number of RF chains set as $N_{\text{RF}} = 4$. We assume that an adequate number of antenna ports are allocated for the FAS at each user, with the number of antenna ports determined by Algorithm 3, utilizing $U = 2N_{\text{RF}}$ and $C^{(N_1 \times N_2)} = C_R$. Consequently, there are $N = 8 \times 8$ antenna ports occupying a physical size of $2\lambda \times 2\lambda$, and $N = 12 \times 12$ ports within $5\lambda \times 5\lambda$ physical size for the FAS. The evaluation of multiplexing gain is conducted as per (28) with the target SINR by (26).

An increase in BICM efficiency implies an increase in the target SINR Γ, which subsequently leads to the increase of outage probability, causing a rapid decrease in multiplexing gain beyond the transmission capability. In addition, we can observe that the multiplexing gain decreases mildly with a low U, indicating that the transmission capability of each UT increases as U decreases. The reason is that the average SINR $\overline{\Gamma} = |\boldsymbol{w}\boldsymbol{y}|^2 / |\boldsymbol{w}\boldsymbol{\eta}^{\text{I}}|^2$ over the block fading channel is inversely related to the number of interferers, $(U-1)$. At a low BICM efficiency, the multiplexing gain in (28) is limited by U, as the target SINR is low and $p_{\text{out}} \to 0$. This observation implies that

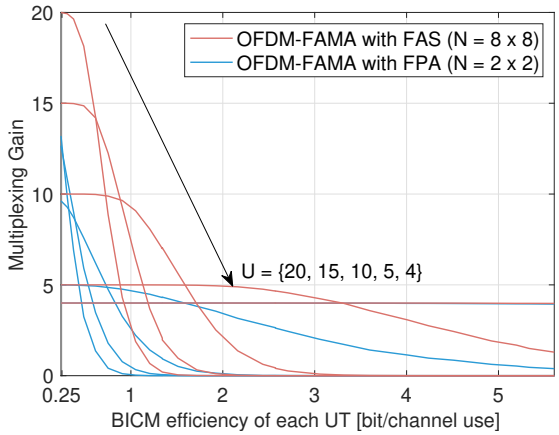

(a) $W = 2 \times 2$

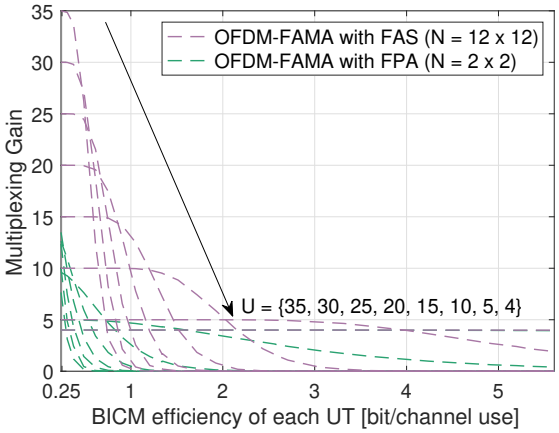

(b) $W = 5 \times 5$

Fig. 6: Multiplexing gains of OFDM-FAMA against the BICM efficiency, with the number of RF chains $N_{\text{RF}} = 4$ and the normalized antenna size: (a) $W = 2 \times 2$, and (b) $W = 5 \times 5$.

the system with robust coding can support a greater number of UTs simultaneously.

Additionally, the multiplexing gains of the system with FPA at each UT are also presented in Fig. 6, with $N = 2 \times 2$ for $N_{\text{RF}} = 4$. It can be observed that the OFDM-FAMA system exhibits superior performance compared to the system with FPA, particularly at low BICM efficiency and large U. But the multiplexing gains converge and become similar as the BICM efficiency increases and U decreases. Notably, when BICM efficiency is lower than 0.5 bit/channel use, the multiplexing gain of the OFDM-FAMA system approaches nearly double that of the system with FPA. This illustrates that the OFDM-FAMA system is particularly suitable for scenarios characterized by a large number of UTs needing to transmit small information packets within the limited spectrum.

V. Link-Level Simulation Results

Link-level simulations are conducted to evaluate the physical layer performance of the OFDM-FAMA system, where U streams are processed in parallel and transmitted by U antennas simultaneously over block fading and TDL-C channel environments. At the u-th UT, a 2D-FAS with $N = N_1 \times N_2$ ports over the normalized size of $W = [W_1, W_2]$ is considered. For the running stage, it is assumed that the FAS can identify and receive signals from the desirable antenna ports. Perfect time synchronization and channel estimation are assumed. The remaining assumptions and parameters we used in the link-level simulations are summarized in Table I. Considering the DMRS overhead in a PRB as $N_{\text{DMRS}} = 12$, the total number of REs allocated for physical downlink share channel (PDSCH) in a subframe is $N_{\text{RE}} = 936$. In the simulations, we adopt the 'short delay spread' defined as in [51, Table 7.7.3-1], such that we have the wanted delay spread $\text{DS}_{\text{desired}} = 30$ ns.

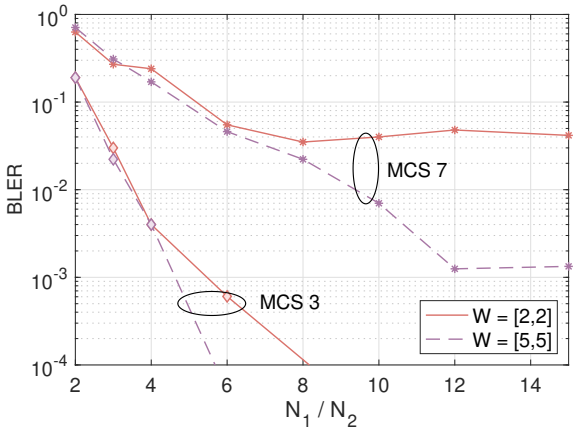

Fig. 7: BLER against the number of antenna ports N_1 (or N_2), with $N_{\text{RF}} = 4$ and $U = 8$, over block fading channels.

We first present the stationary performances of the OFDM-FAMA system during the running stage over the rich-scattering block fading and the TDL-C channels. Then we evaluate the OFDM-FAMA system under mobility situations by link-level simulations over TDL-C channels taking into account varying Doppler frequencies. Specifically, two scenarios are examined: the first scenario represents low-speed conditions, characterized by a velocity of $v = 6.5$ km/h and a corresponding Doppler frequency of $f_D = 30$ Hz; the second scenario reflects high-speed conditions, with $v = 65$ km/h and $f_D = 300$ Hz. The low-speed scenario refers to the pedestrian movement, where speeds typically fluctuate from 0 to 10 km/h, while the high-speed scenario pertains to vehicular movement, where velocities range from 10 to 100 km/h [54]. Finally, the performance of training stage is evaluated.

A. BLER Performance

Fig. 7 demonstrates the BLER results against the number of antenna ports of FAS at each user, utilizing MCS 3 and 7, with $N_{\text{RF}} = 4$ and $U = 8$. MCS 3 and MCS 7 facilitate transmission rate of 0.3 and 0.7 bit/s/Hz for each user, respectively. Block fading channel with rich scattering Rayleigh fading is considered in the results of this figure. As expected, BLER decreases with an increase in the number of antenna ports, N. However, an error floor exists when N is large because of the correlation among the antenna ports within a limited space. This error floor occurs at the lower BLER when the physical size of FAS for each user is increased, or when the channel coding is more robust. These findings are consistent with the semi-analytical evaluations of the rates in Fig. 5.

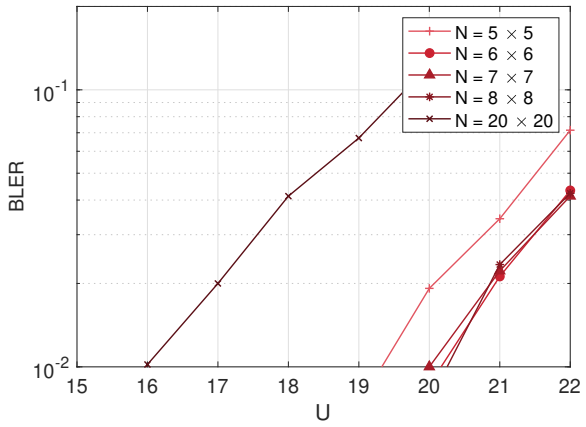

Fig. 8: BLER of MCS 7 against the number of UTs U, with $N_{\text{RF}} = 16$, $W = [2, 2]$ over block fading channels.

TABLE III: FAS configurations at UT of OFDM-FAMA

W	$[2,2]$			$[5,5]$		
N_{RF}	2	4	16	2	4	16
N	10×10	8×8	6×6	15×15	12×12	12×12

Fig. 8 presents the BLER of MCS 7 against the number of users, U, with $N_{\text{RF}} = 16$ and $W = [2, 2]$. As can be seen, the error rate increases with U, since the interference will be more severe with more users. Besides, the FAS configurations of $N = 6 \times 6$, 7×7 or 8×8 can accommodate more UTs while maintaining the same error rate, in contrast to the configurations of $N = 5 \times 5$ or 20×20. The minimum value of N required to achieve the suboptimal performance is $N = 6 \times 6$ for $W = [2, 2]$ and $N_{\text{RF}} = 16$. Also, increasing the antenna ports to 20×20 results in great performance degradation. These observations further align with the semi-analytical evaluations of the achievable rates in Fig. 5.

B. Practical Multiplexing Gain

Here, we conduct the link-level simulations of the suboptimal FAS configuration by Algorithm 3 with $U = 2N_{\text{RF}}$ and $C^{(N_1 \times N_2)} = C_R$. Consequently, the numbers of antenna ports N for different W and N_{RF} are given as in Table III.

The results in Fig. 9 study the BLER of MCS 7 in relation to the number of users U, with different FAS configurations as detailed in Table III. The results of the system with FPA at the UT are also included for comparison. In particular, we focus on identifying the maximum number of users when the BLER is below the threshold of 10^{-2}. This number of users is considered as the practical multiplexing gain, which reflects the connectivity capability of the OFDM-FAMA system. It is evident that the practical multiplexing gain increases when a higher number of RF chains (N_{RF}) and a larger physical size of FAS (W). But the multiplexing gain remains relatively consistent as the physical size W increases when FPA is utilized at the user. The performance enhancements of OFDM-FAMA, compared with the system with FPA, remains remarkable in the multipath channel environment, as shown in Fig. 9(b).

We conduct the link-level simulations for all the MCSs with SEs ranging from 0.16 to 3.75 bit/s/Hz over two channel

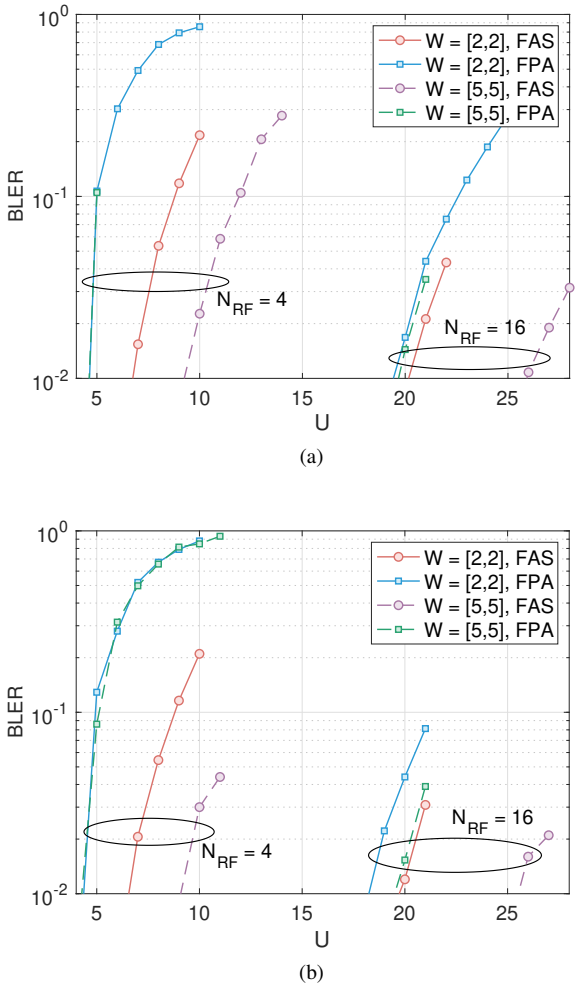

Fig. 9: The BLER performance of MCS7 against the number of UTs U, over (a) block fading, and (b) TDL-C channels.

models. The practical multiplexing gains for block fading and TDL-C are provided in Figs. 10 and 11, respectively. Here, the stationary scenario, with the Doppler frequency $f_d = 0$ Hz, is considered. When $N_{\text{RF}} = 4$, as depicted in Fig. 6(b), the semi-analytical multiplexing gains in Section IV-C are also given as the dotted lines for comparison. The semi-analytical multiplexing gain curves in this figure are derived from the outer envelopes of the multiplexing gain curves with different U in Fig. 6. The BICM efficiency in Fig. 6 is converted to SE in Fig. 10 using

$$\text{SE} = E_{\text{BICM}}(1 - \epsilon_{\text{RS}})(1 - \epsilon_{\text{CP}})(1 - \epsilon_{\text{GB}}), \tag{33}$$

where ϵ_{RS}, ϵ_{CP}, ϵ_{GB} account for the overhead of reference signals, CP, and guard bands (GB), respectively. We observe that the practical multiplexing gain is slightly lower than the semi-analytical gain. This minor gap can be attributed to the rigorous criteria employed in the selection of the threshold, which is BLER $= 10^{-2}$ here.

The results in Figs. 10 and 11 demonstrate that the OFDM-FAMA system offers substantial multiplexing gains when the SE of each UT is relatively low. A multiplexing gain of nearly 80 is achievable at a rate of 0.16 bit/s/Hz, when $N_{\text{RF}} = 16$ and $W = [5, 5]$. The system can obtain a multiplexing gain

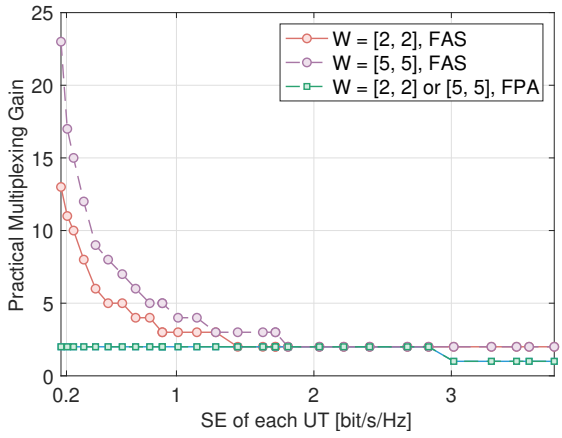

(a)

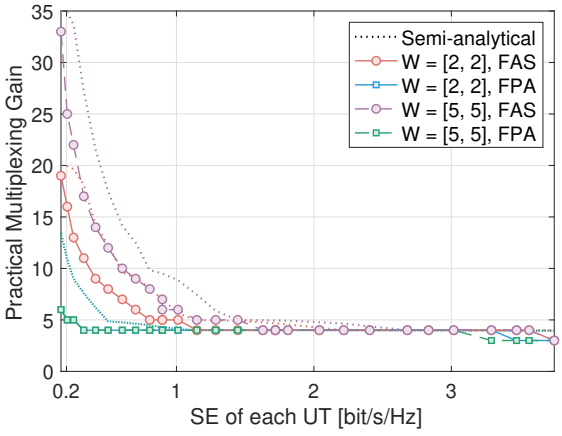

(b)

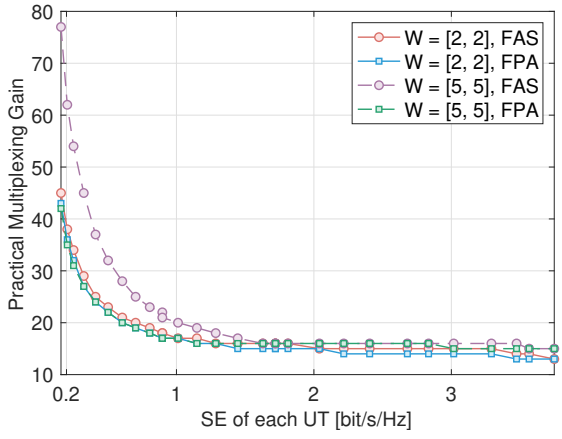

(c)

Fig. 10: Practical multiplexing gains of OFDM-FAMA against the SE over the block fading channel, with (a) $N_{\mathrm{RF}} = 2$, (b) $N_{\mathrm{RF}} = 4$, and (c) $N_{\mathrm{RF}} = 16$.

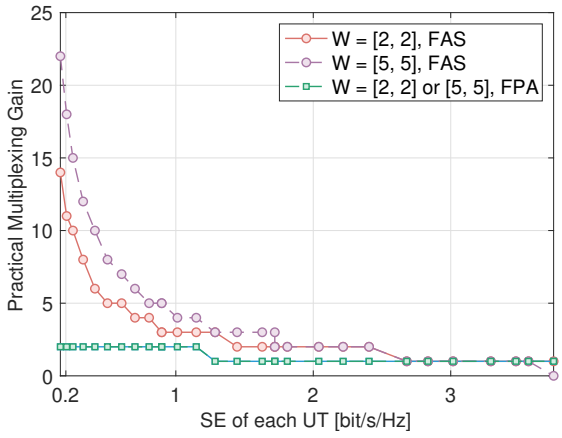

(a)

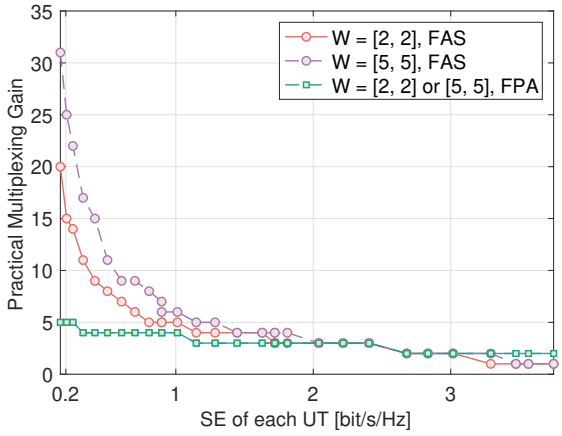

(b)

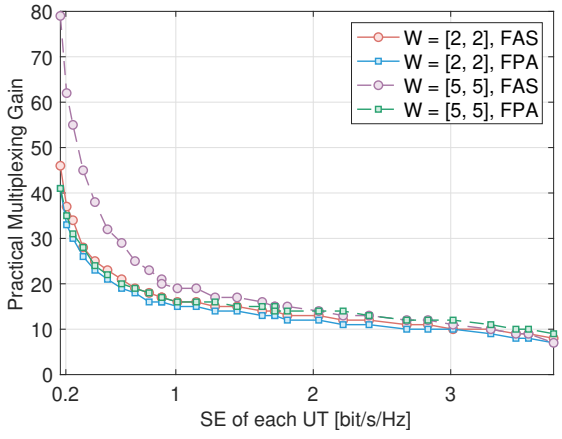

(c)

Fig. 11: Practical multiplexing gains of OFDM-FAMA against the SE over the TDL-C channel, with (a) $N_{\mathrm{RF}} = 2$, (b) $N_{\mathrm{RF}} = 4$, and (c) $N_{\mathrm{RF}} = 16$.

exceeding 50 UTs when using MCS 0-2. Notably, even with a limited number of RF chains at the receiver, the multiplexing gain can exceed 20. This capability facilitates the connectivity of a large number of UTs in a spectrum-limited environment. However, it is observed that the multiplexing gain diminishes as SE increases, ultimately converging around N_{RF}.

In comparison to the system with FPA, the OFDM-FAMA system demonstrates a greater multiplexing gain, particularly when the SE is relatively low. When the receiver at each UT is equipped with a limited number of RF chains, the multiplicative advantages become more pronounced. Specifically, the OFDM-FAMA system yields a ten-fold gain over the system with FPA when $N_{\mathrm{RF}} = 2$, a five-fold gain when $N_{\mathrm{RF}} = 4$, and a two-fold gain when $N_{\mathrm{RF}} = 16$, with $W = [5, 5]$ and adopting MCS 0. Conversely, the numerical value of the multiplexing gain increases as N_{RF} rises. Specifically, the OFDM-FAMA system produces about 20 more multiplexing gain compared to the system with FPA when $N_{\mathrm{RF}} = 2$, about 25 more when $N_{\mathrm{RF}} = 4$, and roughly 40 more when $N_{\mathrm{RF}} = 16$, with $W = [5, 5]$ and MCS 0 adopted. The significant multiplexing gains observed in low SE regions indicate that OFDM-FAMA could serve as a promising technology for mMTC, as mMTC traffic is characterized by low-rate transmissions.

Upon comparing the metrics with $W = [2, 2]$ and $[5, 5]$, we see that an increase in the antenna size does not yield a significant gain in the system with FPA. However, in OFDM-FAMA, a higher practical multiplexing gain is observed with a larger physical size when SE is low. When $W = [2, 2]$ and $N_{\mathrm{RF}} = 16$, the performance of OFDM-FAMA closely resembles that of the FPA-based system. This aligns with the semi-analytical results in Fig. 5. The reason for this similarity is that the FPA MIMO system with $N = 4 \times 4$ receive antennas over a size of $W = 2\lambda \times 2\lambda$ almost approaches the saturation point, thereby exhibiting a relatively high connectivity capability.

Comparing the two channel models, we can first state that their performances are similar at low SE. When SE is elevated, the multiplexing gain over the TDL channel is slightly lower. Also, the range of SE values in which OFDM-FAMA shows a superior multiplexing gain compared to the system using FPA is more extensive within the TDL-C channel.

C. Mobility Evaluation

In order to evaluate the mobility, the TDL-C channel model is used, with the maximum Doppler shift set as 30 Hz for the low-speed scenario and 300 Hz for the high-speed scenario. The practical multiplexing gains for different mobility scenarios are presented in the Tables IV–VI.

The results in the tables indicate that OFDM-FAMA maintains high multiplexing gains with robust MCS at low SE, even in the high-speed scenario. For example, the multiplexing gain of OFDM-FAMA, with UTs with $N_{\mathrm{RF}} = 16$ RF chains and a FAS of ($N = 12 \times 12$, $W = [5, 5]$), remains approximately 80 if MCS 0 is used. Furthermore, OFDM-FAMA can support 25 UTs in the stationary scenario, 26 UTs in the low-speed scenario, and 21 UTs in the high-speed scenario, when MCS 7 with SE $= 0.7$ bit/s/Hz is applied. Besides, OFDM-FAMA continues to provide gains in the mobility scenarios compared

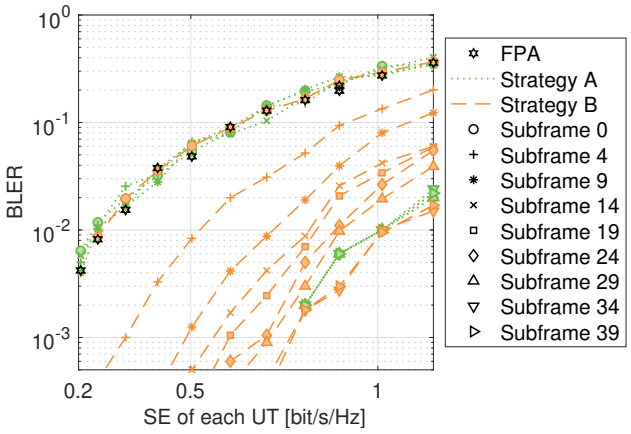

Fig. 12: BLER performances against the SE of OFDM-FAMA for 40 continuous subframes over TDL-C channels, when $U = 5$, $N_{\mathrm{RF}} = 4$, $N = 8 \times 8$, and $W = [2, 2]$.

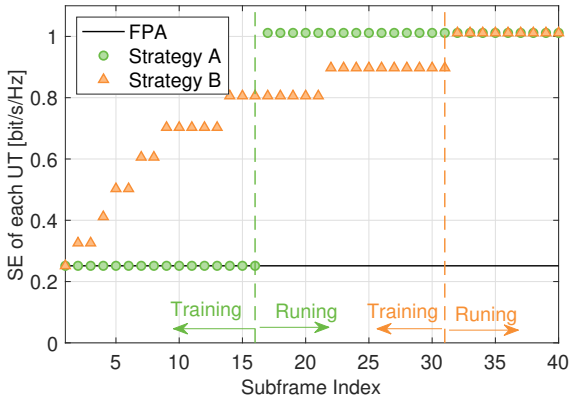

Fig. 13: SE for 40 continuous subframes against the subframe index, over TDL-C channels, when $U = 5$, $N_{\mathrm{RF}} = 4$, $N = 8 \times 8$, and $W = [2, 2]$.

to the FPA-based system, particularly at low SE. Therefore, it can be concluded that the OFDM-FAMA system enhances connectivity through robust channel coding, particularly when the user's receiver possesses ample antenna space albeit a limited number of RF chains. Nonetheless, as the SE increases and high-order modulation is employed, the multiplexing gain diminishes in the stationary scenario, and further declines with increasing Doppler frequency. The observed decline is attributed to the interference present in the system. The SINR threshold for the MCS with a higher modulation order and code rate is higher. As a consequence, with an increased target SINR, the interference will harm the overall capacity. This obervation is consistent with the semi-analytical results in Fig. 6 and the analysis in [9, Fig. 4]. Therefore, to ensure a high multiplexing gain within the system, it is recommended to use low-rate MCS or FAS with configurations that involve large size and/or large number of antenna ports.

D. Performance of Training Stage

Here we evaluate the performance during the training stage with parameters: $N_{\mathrm{RF}} = 4$, $N = 8 \times 8$, and $W = [2, 2]$. The number of subframes designated for training is $N_{\mathrm{subframe}}^{\mathrm{TSA}} = 16$

TABLE IV: Practical multiplexing gains of the OFDM-FAMA system in the stationary scenario when $f_d = 0$ Hz

MCS Index I_{MCS}	Mod. Order Q_m	Target CR $\times 1024$	TBS	SE per UT [bit/s/Hz]	$W = [2, 2]$						$W = [5, 5]$					
					$N_{\text{RF}} = 16$		$N_{\text{RF}} = 4$		$N_{\text{RF}} = 2$		$N_{\text{RF}} = 16$		$N_{\text{RF}} = 4$		$N_{\text{RF}} = 2$	
					FAS	FPA	FAS	FPA	FAS	FPA	FAS	FPA	FAS	FPA	FAS	FPA
0	2	120	224	0.1600	46	41	20	5	15	2	79	41	31	5	22	2
1	2	157	288	0.2057	37	33	15	5	11	2	62	35	25	5	18	2
2	2	193	352	0.2514	34	30	14	5	10	2	55	31	22	5	15	2
3	2	251	456	0.3257	28	26	11	4	8	2	45	28	17	4	12	2
4	2	308	576	0.4114	25	23	9	4	6	2	38	24	15	4	10	2
5	2	379	704	0.5028	23	21	8	4	5	2	32	22	11	4	8	2
6	2	449	848	0.6057	21	19	7	4	5	2	29	20	9	4	7	2
7	2	526	984	0.7028	19	18	6	4	4	2	25	19	9	4	6	2
8	2	602	1128	0.8057	18	16	5	4	4	2	23	18	8	4	5	2
9	2	679	1256	0.8971	17	16	5	4	3	2	21	17	7	4	5	2
10	4	340	1256	0.8971	17	16	5	4	3	2	20	17	6	4	5	2
11	4	378	1416	1.0114	16	15	5	4	3	2	19	16	6	4	4	2
12	4	434	1608	1.1486	16	15	4	3	3	2	19	16	5	3	4	2
13	4	490	1800	1.2857	15	14	4	3	3	1	17	16	5	3	3	1
14	4	553	2024	1.4457	15	14	4	3	2	1	17	15	4	3	3	1
15	4	616	2280	1.6285	14	13	4	3	2	1	16	15	4	3	3	1
16	4	658	2408	1.7200	14	13	3	3	2	1	15	15	4	3	3	1
17	6	438	2408	1.7200	14	13	3	3	2	1	15	14	4	3	2	1
18	6	466	2536	1.8114	13	12	3	3	2	1	15	14	4	3	2	1
19	6	517	2856	2.0400	13	12	3	3	2	1	14	14	3	3	2	1
20	6	567	3104	2.2171	12	11	3	3	2	1	13	14	3	3	2	1
21	6	616	3368	2.4057	12	11	3	3	2	1	13	13	3	3	2	1
22	6	666	3752	2.6800	11	10	2	2	1	1	12	12	2	2	1	1
23	6	719	3968	2.8342	11	10	2	2	1	1	12	12	2	2	1	1
24	6	772	4224	3.0171	10	10	2	2	1	1	11	12	2	2	1	1
25	6	822	4608	3.2914	10	9	1	2	1	1	10	11	2	2	1	1
26	6	873	4864	3.4743	9	8	1	2	1	1	9	10	1	2	1	1
27	6	910	4992	3.5657	9	8	1	2	1	1	9	10	1	2	1	1
28	6	948	5248	3.7486	8	7	1	2	1	1	7	9	1	2	0	1

Note that the grey-shaded cells indicate the cases where FAS does not outperform FPA.

TABLE V: Practical multiplexing gains of the OFDM-FAMA system in the low-speed scenario when $f_d = 30$ Hz

MCS Index I_{MCS}	Mod. Order Q_m	Target CR $\times 1024$	TBS	SE per UT [bit/s/Hz]	$W = [2, 2]$						$W = [5, 5]$					
					$N_{\text{RF}} = 16$		$N_{\text{RF}} = 4$		$N_{\text{RF}} = 2$		$N_{\text{RF}} = 16$		$N_{\text{RF}} = 4$		$N_{\text{RF}} = 2$	
					FAS	FPA	FAS	FPA	FAS	FPA	FAS	FPA	FAS	FPA	FAS	FPA
0	2	120	224	0.1600	46	41	20	6	14	2	80	42	32	6	21	2
1	2	157	288	0.2057	39	34	16	5	11	2	63	35	25	5	17	2
2	2	193	352	0.2514	35	30	14	5	10	2	53	31	21	5	17	2
3	2	251	456	0.3257	29	26	11	4	8	2	46	28	17	4	11	2
4	2	308	576	0.4114	25	23	9	4	6	2	36	24	14	4	9	2
5	2	379	704	0.5028	22	20	8	4	5	2	33	22	11	4	8	2
6	2	449	848	0.6057	20	18	7	4	5	2	28	20	10	4	7	2
7	2	526	984	0.7028	19	18	6	4	4	2	26	19	8	4	6	2
8	2	602	1128	0.8057	18	17	6	4	4	2	23	18	8	4	5	2
9	2	679	1256	0.8971	17	16	5	4	3	2	21	17	7	3	5	2
10	4	340	1256	0.8971	17	16	5	4	3	2	21	17	7	3	5	1
11	4	378	1416	1.0114	16	15	4	3	3	1	19	16	6	3	4	1
12	4	434	1608	1.1486	16	14	4	3	3	1	18	16	5	3	4	1
13	4	490	1800	1.2857	15	14	4	3	3	1	17	15	5	3	3	1
14	4	553	2024	1.4457	14	13	4	3	2	1	16	15	5	3	3	1
15	4	616	2280	1.6285	14	13	3	3	2	1	16	14	4	3	3	1
16	4	658	2408	1.7200	14	13	3	3	2	1	15	14	4	3	3	1
17	6	438	2408	1.7200	13	12	3	3	2	1	15	14	4	3	2	1
18	6	466	2536	1.8114	13	12	3	3	2	1	14	14	4	3	2	1
19	6	517	2856	2.0400	12	12	3	3	2	1	14	13	3	3	2	1
20	6	567	3104	2.2171	12	11	3	3	2	1	13	13	3	3	2	1
21	6	616	3368	2.4057	12	10	3	2	1	1	13	12	3	3	2	1
22	6	666	3752	2.6800	11	10	2	2	1	1	12	12	2	2	1	1
23	6	719	3968	2.8342	10	10	2	2	1	1	11	12	2	2	1	1
24	6	772	4224	3.0171	10	9	2	2	1	1	11	11	2	2	1	1
25	6	822	4608	3.2914	9	8	2	2	1	1	10	11	2	2	1	1
26	6	873	4864	3.4743	8	8	1	2	1	1	9	9	1	2	1	1
27	6	910	4992	3.5657	8	7	1	2	1	1	8	9	1	2	1	1
28	6	948	5248	3.7586	7	7	1	2	1	1	7	8	1	2	0	1

Note that the grey-shaded cells indicate the cases where FAS does not outperform FPA.

TABLE VI: Practical multiplexing gains of the OFDM-FAMA system in the high-speed scenario when $f_d = 300$ Hz

MCS Index I_{MCS}	Mod. Order Q_m	Target CR $\times 1024$	TBS	SE per UT [bit/s/Hz]	$W = [2,2]$						$W = [5,5]$					
					$N_{\text{RF}} = 16$		$N_{\text{RF}} = 4$		$N_{\text{RF}} = 2$		$N_{\text{RF}} = 16$		$N_{\text{RF}} = 4$		$N_{\text{RF}} = 2$	
					FAS	FPA	FAS	FPA	FAS	FPA	FAS	FPA	FAS	FPA	FAS	FPA
0	2	120	224	0.1600	44	41	18	6	11	2	80	41	31	6	18	2
1	2	157	288	0.2057	37	33	14	5	9	2	56	35	22	5	14	2
2	2	193	352	0.2514	32	29	12	4	8	1	52	30	19	4	12	1
3	2	251	456	0.3257	28	24	10	4	6	1	42	25	16	3	10	1
4	2	308	576	0.4114	23	21	8	3	5	1	35	23	12	3	8	1
5	2	379	704	0.5028	20	18	7	3	4	1	29	19	10	3	6	1
6	2	449	848	0.6057	18	16	6	3	4	1	24	17	9	3	5	1
7	2	526	984	0.7028	16	14	5	3	3	1	21	15	7	3	4	1
8	2	602	1128	0.8057	14	13	5	3	3	1	19	14	7	3	4	1
9	2	679	1256	0.8971	13	12	4	2	3	1	18	13	6	2	4	1
10	4	340	1256	0.8971	13	12	4	2	3	1	17	13	5	2	4	1
11	4	378	1416	1.0114	12	11	4	2	2	1	16	12	5	2	3	1
12	4	434	1608	1.1486	11	10	3	2	2	1	14	11	4	2	3	1
13	4	490	1800	1.2857	10	10	3	2	2	1	13	11	4	2	2	1
14	4	553	2024	1.4457	9	9	3	2	2	1	12	10	3	2	2	1
15	4	616	2280	1.6285	9	8	3	2	2	1	11	9	3	2	2	1
16	4	658	2408	1.7200	9	8	2	2	2	1	10	9	3	2	2	1
17	6	438	2408	1.7200	8	8	2	2	1	1	10	9	3	2	2	1
18	6	466	2536	1.8114	8	8	2	2	1	1	10	9	3	2	2	1
19	6	517	2856	2.0400	7	7	2	2	1	1	9	8	2	2	2	1
20	6	567	3104	2.2171	7	7	2	2	1	1	8	8	2	2	1	1
21	6	616	3368	2.4057	7	6	2	2	1	1	8	8	2	2	1	1
22	6	666	3752	2.6800	6	6	2	2	1	1	7	7	2	2	1	1
23	6	719	3968	2.8342	6	6	2	1	1	1	7	7	2	2	1	1
24	6	772	4224	3.0171	6	5	1	1	1	1	6	7	1	1	1	1
25	6	822	4608	3.2914	5	5	1	1	1	1	6	6	1	1	1	1
26	6	873	4864	3.4743	5	5	1	1	1	1	5	6	1	1	1	1
27	6	910	4992	3.5657	5	5	1	1	1	1	5	6	1	1	0	1
28	6	948	5248	3.7586	4	4	1	1	0	0	4	5	1	1	0	0

Note that the grey-shaded cells indicate the cases where FAS does not outperform FPA.

for *Strategy A*, and $N_{\text{subframe}}^{\text{TSB}} = 31$ for *Strategy B*. We simulate 40 continuous subframes with $U = 5$ UTs in the OFDM-FAMA system. The BLERs of these continuous subframes are illustrated in Fig. 12, against the SE per UT under different MCSs. As we can observe, the BLER during the training stage is inferior to that of the running stage, indicating that the system needs to operate at a low rate during the training stage, and the rate could subsequently be increased during the running stage. The curves of *Strategy A* are categorized into two distinct clusters. The first cluster pertains to the subframes within the training stage, i.e., $n_{\text{subframe}} < N_{\text{subframe}}^{\text{TSA}}$, where their performance aligns with that of the FPA-based system. The second cluster corresponds to the subframes in the running stage, i.e., $n_{\text{subframe}} \geq N_{\text{subframe}}^{\text{TSA}}$, where the BLER performance is significantly enhanced compared to the training stage. In the case of *Strategy B*, the performance of the first subframe ($n_{\text{subframe}} = 0$) is the same as that of the system with FPA, and continuous improvement in the performance is noted as n_{subframe} increases. This occurs because *Strategy B* selects half of the RF chains from the known good antenna ports.

With the BLER threshold of 10^{-2}, we present the SE of 40 simulated continuous subframes in relation to the subframe index in Fig. 13. It clearly shows the significant improvements in transmission rate between the training and running stages of the two proposed strategies. For *Strategy A*, the data rate remains at a low level of approximately 0.2 bit/s/Hz during the training stage, subsequently improving to 1 bit/s/Hz during the running stage. In contrast, *Strategy B* demonstrates an enhancement in data rate from 0.2 to 1.0 bit/s/Hz throughout its training stage.

VI. Conclusion

In this paper, we proposed the OFDM-FAMA system, using the 5G NR numerology and channel coding. The average SINR of a subframe serves as a key metric for selecting the ports for FAMA, and we proposed the port selector with two training strategies. IRC equalization was employed to further mitigate the interference at the receiver. We derived and conducted the analysis of the outage rate, channel capacity, and cutoff rate, and proposed an algorithm to find the suboptimal configuration of FAS at the UT based on these rates. Link-level results in this paper confirmed the suboptimal N^* identified through the proposed algorithm yields superior BLER performance with a minimal number of ports. Furthermore, extensive simulation results indicated that the OFDM-FAMA could support a significant number of UTs with robust channel coding.

References

[1] N. H. Mahmood *et al.*, "Six key features of machine type communication in 6G," *The 2nd 6G Wireless Summit (6G SUMMIT)*, pp. 1–5, 17-20 May 2020, Levi, Finland.

[2] X. Chen *et al.*, "Massive access for 5G and beyond," *IEEE J. Select. Areas Commun.*, vol. 39, no. 3, pp. 615–637, Mar. 2021.

[3] H. Q. Ngo, G. Interdonato, E. G. Larsson, G. Caire and J. G. Andrews, "Ultradense cell-free massive MIMO for 6G: Technical overview and open questions," *Proc. IEEE*, vol. 112, no. 7, pp. 805–831, Jul. 2024.

[4] Z. Wang *et al.*, "Extremely large-scale MIMO: Fundamentals, challenges, solutions, and future directions," *IEEE Wireless Commun.*, vol. 31, no. 3, pp. 117–124, Jun. 2024.

[5] F. A. Pereira de Figueiredo, "An overview of massive MIMO for 5G and 6G," *IEEE Latin America Trans.*, vol. 20, no. 6, pp. 931–940, Jun. 2022.

[6] A. Ahmed *et al.*, "Unveiling the potential of NOMA: A journey to next generation multiple access," *IEEE Commun. Surv. & Tut.*, doi:10.1109/COMST.2024.3521647, 2024.

[7] L. Dai *et al.*, "A survey of non-orthogonal multiple access for 5G," *IEEE Commun. Surv. & Tut.*, vol. 20, no. 3, pp. 2294–2323, Thirdquarter 2018.

[8] Y. Mao *et al.*, "Rate-splitting multiple access: Fundamentals, survey, and future research trends," *IEEE Commun. Surv. & Tut.*, vol. 24, no. 4, pp. 2073–2126, Fourthquarter 2022.

[9] K. K. Wong and K. F. Tong, "Fluid antenna multiple access," *IEEE Trans. Wireless Commun.*, vol. 21, no. 7, pp. 4801–4815, Jul. 2022.

[10] W. K. New *et al.*, "A tutorial on fluid antenna system for 6G networks: Encompassing communication theory, optimization methods and hardware designs," *IEEE Commun. Surv. & Tutor.*, doi:10.1109/COMST.2024.3498855, 2024.

[11] K. K. Wong, K. F. Tong, Y. Zhang, and Z. Zheng, "Fluid antenna system for 6G: When Bruce Lee inspires wireless communications," *Elect. Lett.*, vol. 56, no. 24, pp. 1288–1290, Nov. 2020.

[12] K. K. Wong, A. Shojaeifard, K. F. Tong, and Y. Zhang, "Fluid antenna systems," *IEEE Trans. Wireless Commun.*, vol. 20, no. 3, pp. 1950–1962, Mar. 2021.

[13] Y. Huang, L. Xing, C. Song, S. Wang and F. Elhouni, "Liquid antennas: Past, present and future," *IEEE Open J. Antennas & Propag.*, vol. 2, pp. 473–487, Mar. 2021.

[14] K. N. Paracha, A. D. Butt, A. S. Alghamdi, S. A. Babale, and P. J. Soh, "Liquid metal antennas: Materials, fabrication and applications," *Sensors*, vol. 20, no. 1, p. 177, Dec. 2019.

[15] Y. Shen *et al.*, "Design and implementation of mmWave surface wave enabled fluid antennas and experimental results for fluid antenna multiple access," *arXiv preprint*, arXiv:2405.09663, May 2024.

[16] T. V. Hoang, V. Fusco, T. Fromenteze and O. Yurduseven, "Computational polarimetric imaging using two-dimensional dynamic metasurface apertures," *IEEE Open J. Antennas & Propag.*, vol. 2, pp. 488–497, Mar. 2021.

[17] J. Zhang *et al.*, "A novel pixel-based reconfigurable antenna applied in fluid antenna systems with high switching speed," *IEEE Open J. Antennas & Propag.*, vol. 6, no. 1, pp. 212–228, Feb. 2025.

[18] S. Basbug, "Design and synthesis of antenna array with movable elements along semicircular paths," *IEEE Antennas Wireless Propag. Lett.*, vol. 16, pp. 3059–3062, Oct. 2017.

[19] M. C. Johnson, S. L. Brunton, N. B. Kundtz, and J. N. Kutz, "Sidelobe canceling for reconfigurable holographic metamaterial antenna," *IEEE Trans. Antennas & Propag.*, vol. 63, no. 4, pp. 1881–1886, Apr. 2015.

[20] M. Khammassi, A. Kammoun and M.-S. Alouini, "A new analytical approximation of the fluid antenna system channel," *IEEE Trans. Wireless Commun.*, vol. 22, no. 12, pp. 8843–8858, Dec. 2023.

[21] J. D. Vega-Sánchez, A. E. López-Ramírez, L. Urquiza-Aguiar, and D. P. M. Osorio, "Novel expressions for the outage probability and diversity gains in fluid antenna system," *IEEE Wireless Commun. Lett.*, vol. 13, no. 2, pp. 372–376, Feb. 2024.

[22] J. D. Vega-Sánchez, L. Urquiza-Aguiar, M. C. P. Paredes, and D. P. M. Osorio, "A simple method for the performance analysis of fluid antenna systems under correlated Nakagami-m fading," *IEEE Wireless Commun. Lett.*, vol. 13, no. 2, pp. 377–381, Feb. 2024.

[23] P. D. Alvim *et al.*, "On the performance of fluid antennas systems under α-μ fading channels," *IEEE Wireless Commun. Lett.*, vol. 13, no. 1, pp. 108–112, Jan. 2024.

[24] C. Psomas, P. J. Smith, H. A. Suraweera, and I. Krikidis, "Continuous fluid antenna systems: Modeling and analysis," *IEEE Commun. Lett.*, vol. 27, no. 12, pp. 3370–3374, Dec. 2023.

[25] W. K. New, K. K. Wong, H. Xu, K. F. Tong and C. B. Chae, "Fluid Antenna System: New Insights on Outage Probability and Diversity Gain," *IEEE Trans. Wireless Commun.*, vol. 23, no. 1, pp. 128–140, Jan. 2024.

[26] L. Zhu and K.-K. Wong, "Historical review of fluid antennas and movable antennas," *ArXiv preprint*, arXiv:2401.02362, Jan. 2024.

[27] C. Skouroumounis and I. Krikidis, "Fluid antenna with linear MMSE channel estimation for large-scale cellular networks," *IEEE Trans. Commun.*, vol. 71, no. 2, pp. 1112–1125, Feb. 2023.

[28] H. Xu *et al.*, "Channel estimation for FAS-assisted multiuser mmWave systems," *IEEE Commun. Lett.*, vol. 28, no. 3, pp. 632–636, Mar. 2024.

[29] Z. Zhang, J. Zhu, L. Dai, and R. W. Heath Jr, "Successive Bayesian reconstructor for channel estimation in fluid antenna systems," *arXiv preprint*, arXiv:2312.06551v3, 2024.

[30] W. K. New, K. K. Wong, H. Xu, K. F. Tong, and C.-B. Chae, "An information-theoretic characterization of MIMO-FAS: Optimization, diversity-multiplexing tradeoff and q-outage capacity," *IEEE Trans. Wireless Commun.*, vol. 23, no. 6, pp. 5541–5556, Jun. 2024.

[31] L. Zhou, J. Yao, M. Jin, T. Wu and K. K. Wong, "Fluid antenna-assisted ISAC systems," *IEEE Wireless Commun. Lett.*, vol. 13, no. 12, pp. 3533–3537, Dec. 2024.

[32] C. Skouroumounis and I. Krikidis, "Fluid antenna-aided full duplex communications: A macroscopic point-of-view," *IEEE J. Select. Areas Commun.*, vol. 41, no. 9, pp. 2879–2892, Sept. 2023.

[33] S. Ye, D. Zhang, M. Xiao and M. Skoglund, "Integrated communication and computation empowered by fluid antenna array," in *Proc. IEEE Int. Workshop Sig. Process. Adv. Wireless Commun. (SPAWC)*, pp. 276–280, 10-13 Sept. 2024, Lucca, Italy.

[34] P. Mursia *et al.*, "T3DRIS: Advancing conformal RIS design through in-depth analysis of mutual coupling effects," *IEEE Trans. Commun.*, vol. 73, no. 2, pp. 889–903, Feb. 2025.

[35] X. Shao, Q. Jiang and R. Zhang, "6D movable antenna based on user distribution: Modeling and optimization," *IEEE Trans. Wireless Commun.*, vol. 24, no. 1, pp. 355–370, Jan. 2025.

[36] X. Shao, R. Zhang, Q. Jiang and R. Schober, "6D movable antenna enhanced wireless network via discrete position and rotation optimization," *IEEE J. Sel. Areas Commun.*, vol. 43, no. 3, pp. 674–687, Mar. 2025.

[37] K. K. Wong, K. F. Tong, Y. Chen, and Y. Zhang, "Fast fluid antenna multiple access enabling massive connectivity," *IEEE Commun. Lett.*, vol. 27, no. 2, pp. 711–715, Feb. 2023.

[38] K. K. Wong, D. Morales-Jimenez, K. F. Tong, and C. B. Chae, "Slow fluid antenna multiple access," *IEEE Trans. Commun.*, vol. 71, no. 5, pp. 2831–2846, May 2023.

[39] K. K. Wong, C. B. Chae, and K. F. Tong, "Compact ultra massive antenna array: A simple open-loop massive connectivity scheme," *IEEE Trans. Wireless Commun.*, vol. 23, no. 6, pp. 6279–6294, Jun. 2024.

[40] K. K. Wong, "Transmitter CSI-free RIS-randomized CUMA for extreme massive connectivity," *IEEE Open J. Commun. Soc.*, vol. 5, pp. 6890–6902, Oct. 2024.

[41] P. Ramírez-Espinosa, D. Morales-Jimenez and K. K. Wong, "A new spatial block-correlation model for fluid antenna systems," *IEEE Trans. Wireless Commun.*, vol. 23, no. 11, pp. 15829–15843, Nov. 2024.

[42] H. Xu *et al.*, "Revisiting outage probability analysis for two-user fluid antenna multiple access system," *IEEE Trans. Wireless Commun.*, vol. 23, no. 8, pp. 9534–9548, Aug. 2024.

[43] N. Waqar, K. K. Wong, K. F. Tong, A. Sharples, and Y. Zhang, "Deep learning enabled slow fluid antenna multiple access," *IEEE Commun. Lett.*, vol. 27, no. 3, pp. 861–865, Mar. 2023.

[44] H. Hong, K. K. Wong, K. F. Tong, H. Shin, and Y. Zhang, "Coded fluid antenna multiple access over fast fading channels," *IEEE Wireless Commun. Lett.*, doi:10.1109/LWC.2025.3540668, 2025.

[45] H. Hong, K. K. Wong, K. F. Tong, H. Xu, and H. Li, "5G-coded fluid antenna multiple access over block fading channels," *IET Elect. Lett.*, doi:10.22541/au.173200600.04553159/v1, 2024.

[46] J. Yli-Kaakinen *et al.*, "Frequency-domain signal processing for spectrally-enhanced CP-OFDM waveforms in 5G new radio," *IEEE Trans. Wireless Commun.*, vol. 20, no. 10, pp. 6867–6883, Oct. 2021.

[47] L. Zhu, W. Ma, Z. Xiao and R. Zhang, "Performance Analysis and Optimization for Movable Antenna Aided Wideband Communications," IEEE Trans. Wireless Commun., vol. 23, no. 12, pp. 18653–18668, Dec. 2024.

[48] "NR; Physical layer procedures for data," Available [Online]: https://www.3gpp.org/ftp/Specs/archive/38_series/38.214/38214-i40.zip, Last Accessed on 2024-09-23.

[49] "NR; Multiplexing and channel coding," Available [Online]: https://www.3gpp.org/ftp/Specs/archive/38_series/38.212/38212-i40.zip, Last Accessed on 2024-09-23.

[50] "NR; Physical channels and modulation," Available [Online]: https://www.3gpp.org/ftp/Specs/archive/38_series/38.211/38211-i40.zip, Last Accessed on 2024-09-23.

[51] "Study on channel model for frequencies from 0.5 to 100 GHz," Available [Online]: https://www.3gpp.org/ftp/Specs/archive/38_series/38.901/8901-i00.zip, Last Accessed on 2024-04-03.

[52] "Evolved universal terrestrial radio access (E-UTRA); User equipment (UE) radio transmission and reception," Available [Online]: https://www.3gpp.org/ftp/Specs/archive/36_series/36.101/36101-j01.zip, Last Accessed on 2025-01-11.

[53] Y. S. Cho *et al.* "MIMO-OFDM wireless communications with MATLAB," *John Wiley & Sons*, 2010.

[54] “D2.1 Use Case story definition, requirements and KPIs” Available [Online]: https://www.5g-records.eu/Deliverables/5G-RECORDS_D2.1_v2.0_web.pdf, Last Accessed on 2022-01-21.